Study of Υ production in pPb collisions at $\sqrt{s_{NN}}=8.16$ TeV

Citation for published version:
Clarke, P, Cowan, G, Eisenhardt, S, Gambetta, S, Muheim, F, Needham, M, Pappagallo, M, Playfer, S, Williams, M & Collaboration, LHC 2018, 'Study of Υ production in pPb collisions at $\sqrt{s_{NN}}=8.16$ TeV', *Journal of High Energy Physics*, vol. 1811, 194. https://doi.org/10.1007/JHEP11(2018)194

Digital Object Identifier (DOI):
10.1007/JHEP11(2018)194

Link:
Link to publication record in Edinburgh Research Explorer

Document Version:
Publisher's PDF, also known as Version of record

Published In:
Journal of High Energy Physics

Published for SISSA by Springer

Received: *October 18, 2018*
Accepted: *November 20, 2018*
Published: *November 29, 2018*

Study of Υ production in pPb collisions at $\sqrt{s_{\rm NN}} = 8.16$ TeV

The LHCb collaboration

E-mail: shanzhen.chen@cern.ch

Abstract: The production of $\Upsilon(nS)$ mesons ($n = 1, 2, 3$) in pPb and Pbp collisions at a centre-of-mass energy per nucleon pair $\sqrt{s_{\rm NN}} = 8.16\,\text{TeV}$ is measured by the LHCb experiment, using a data sample corresponding to an integrated luminosity of $31.8\,\text{nb}^{-1}$. The $\Upsilon(nS)$ mesons are reconstructed through their decays into two opposite-sign muons. The measurements comprise the differential production cross-sections of the $\Upsilon(1S)$ and $\Upsilon(2S)$ states, their forward-to-backward ratios and nuclear modification factors. The measurements are performed as a function of the transverse momentum $p_{\rm T}$ and rapidity in the nucleon-nucleon centre-of-mass frame y^* of the $\Upsilon(nS)$ states, in the kinematic range $p_{\rm T} < 25\,\text{GeV}/c$ and $1.5 < y^* < 4.0$ ($-5.0 < y^* < -2.5$) for pPb (Pbp) collisions. In addition, production cross-sections for $\Upsilon(3S)$ are measured integrated over phase space and the production ratios between all three $\Upsilon(nS)$ states are determined. Suppression for bottomonium in proton-lead collisions is observed, which is particularly visible in the ratios. The results are compared to theoretical models.

Keywords: Heavy Ion Experiments

ArXiv ePrint: 1810.07655

https://doi.org/10.1007/JHEP11(2018)194

Contents

1 Introduction

Existing experimental results in collisions of ultra-relativistic heavy nuclei are consistent with the formation of a deconfined state of hot partonic matter, referred to as Quark-Gluon Plasma (QGP) [1, 2]. One of the signatures of QGP is the suppression of heavy-quarkonia production in the collisions of heavy nuclei (AA collisions) with respect to pp collisions, an effect that is enhanced for states with lower binding energies, such as the $\Upsilon(3S)$ meson [3]. However, the suppression of heavy-quarkonia production can also occur in the collisions of protons with heavy nuclei (pA collisions), where traditionally it was assumed that there was no QGP created.

In pA collisions, this suppression is caused by nuclear phenomena unrelated to deconfinement, commonly called cold nuclear matter (CNM) effects. The CNM effects that are expected to affect quarkonia production are of two types, "initial-state" effects happening at a early stage of the collision, such as nuclear effects on parton densities [4–7] or coherent energy losses [8–10], and "final-state" effects, as quarkonia absorption by nucleons [11], expected to be negligible at LHC energies [12–15]. Another final-state effect is the breaking of the $q\bar{q}$ pair caused by collisions with comoving particles with similar rapidities (the so-called "comovers" model [16–20]), whose density is determined from the particle multiplicity measured in that region of rapidity. This model could explain the relative suppression observed among the $\Upsilon(nS)$ states both in AA [21] and in pA collisions [22]. The size of nuclear effects can be quantified by measuring the nuclear modification factor R_{pA}, which is defined as the ratio of the cross-section in pA collisions to that in pp collisions scaled by the number of nucleons in the nucleus. In the absence of modifications, R_{pA} is unity.

Previous measurements in pA and AA collisions at RHIC [23] and LHC [22, 24–27] have revealed sizable nuclear modification factors for the $\Upsilon(nS)$ states and a suppression which seems to be more pronounced for the higher states. Using a data sample corresponding to an integrated luminosity of about $1.5\,\text{nb}^{-1}$, the LHCb collaboration measured the production of $\Upsilon(nS)$ mesons in pPb collisions at a per-nucleon centre-of-mass energy of $\sqrt{s_{\text{NN}}} = 5\,\text{TeV}$ [28]. Moreover, the measurement of nuclear modification and forward-backward production ratios for $\Upsilon(1S)$, as well as $\Upsilon(nS)$ to $\Upsilon(1S)$ ratios, were performed.

In this paper, the production of $\Upsilon(nS)$ mesons is studied in pPb collisions using data collected at $\sqrt{s_{\text{NN}}} = 8.16\,\text{TeV}$ with the LHCb detector, corresponding to a total integrated luminosity of $31.8\,\text{nb}^{-1}$. This dataset has been used already for the study of the production of prompt J/ψ and J/ψ coming from b-hadron decays (called nonprompt J/ψ in the following) [29]. The measurements presented in this work comprise the differential production cross-sections of the $\Upsilon(1S)$ and $\Upsilon(2S)$ states, their forward-to-backward ratios and nuclear modification factors, and the production ratios between all three $\Upsilon(nS)$ states. In addition, the ratio of $\Upsilon(1S)$ to nonprompt J/ψ cross-sections is determined as a function of proton-nucleon centre-of-mass rapidity, y^*, integrated over the transverse momenta, p_{T}, of the mesons, a measurement that allows direct comparison of open heavy-flavour and quarkonia production in the environment of heavy-nuclei collisions.

2 Detector description and data samples

The LHCb detector [30, 31] is a single-arm forward spectrometer designed for the study of particles containing b or c quarks. The detector includes a high-precision tracking system consisting of a silicon-strip vertex detector surrounding the beam-beam interaction region [32], a large-area silicon-strip detector located upstream of a dipole magnet with a bending power of about 4 Tm, and three stations of silicon-strip detectors and straw drift tubes [33] placed downstream of the magnet. The tracking system provides a measurement of the momentum of charged particles with a relative uncertainty that varies from 0.5% at low momentum to 1.0% at $200\,\text{GeV}/c$. The minimum distance of a track to a primary vertex (PV), the impact parameter (IP), is measured with a resolution of $(15 + 29/p_{\text{T}})\,\mu\text{m}$, where p_{T} is in GeV/c. Different types of charged hadrons are distinguished using information from two ring-imaging Cherenkov detectors [34]. Photons, electrons and hadrons are identified by a calorimeter system consisting of scintillating-pad and preshower detectors, an electromagnetic calorimeter and a hadronic calorimeter. Muons are identified by a system composed of alternating layers of iron and multiwire proportional chambers [35].

The trigger [36] consists of a hardware stage, based on information from the calorimeter and muon systems, followed by a software stage, in which all charged particles with $p_{\mathrm{T}} > 300\,\mathrm{MeV}/c$ are reconstructed. The alignment and calibration of the detector is performed in near real-time [37]. This alignment is also used later in the offline reconstruction, ensuring consistent and high-quality particle identification (PID) information in the online and offline processing. The identical performance of the online and offline reconstruction offers the opportunity to perform physics analyses directly using candidates reconstructed in the trigger [36, 38] as well as storing information about all reconstructed particles in the event [39]. The storage of only the triggered candidates enables a reduction of the event size by an order of magnitude.

For this analysis, at least one muon with $p_{\mathrm{T}} > 500\,\mathrm{MeV}/c$ is required at the hardware trigger stage and at the software trigger stage, two muon tracks with $p_{\mathrm{T}} > 300\,\mathrm{MeV}/c$ and a high-quality reconstructed decay vertex are required to form an $\Upsilon(nS)$ candidate with invariant mass $m(\mu^+\mu^-) > 4.7\,\mathrm{GeV}/c^2$. In addition, a small fraction of events with a large number of tracks in the vertex detector are rejected to avoid potential problems at the reconstruction stage.

Simulation is used in the determination of efficiencies. The pPb collisions are simulated with EPOS-LHC [40] and the $\Upsilon(nS) \to \mu^+\mu^-$ decays with Pythia 8.1 [41, 42] in pp collisions where the proton energy is equal to that in pPb collisions. The interaction of the generated particles with the detector and its response are implemented using the Geant4 toolkit [43, 44], as described in ref. [45]. The $\Upsilon(nS)$ mesons are produced unpolarised, justified by the fact that the polarisation of $\Upsilon(nS)$ mesons has been measured by LHCb in pp collisions at similar energies and found to be small [46]. Consistently with what was done in previous LHCb analyses [29], no systematic uncertainty is associated with this assumption.

The asymmetric layout of the LHCb experiment [30], which covers the pseudorapidity range of $2 < \eta < 5$, results in two configurations: in the *forward* pPb (*backward* Pbp) configuration, the proton (lead) beam travels from the VELO detector to the muon chambers, taking advantage of the inversion of the proton and lead beams during the pPb data-taking run. The energy of the proton beam is 6.5 TeV, while that of the lead beam is 2.56 TeV per nucleon, resulting in a centre-of-mass energy of the proton-nucleon system of 8.16 TeV . Since the energy per nucleon in the proton beam is significantly larger than that in the lead beam, the proton-nucleon centre-of-mass system has a rapidity in the laboratory frame of +0.465 (−0.465) for pPb (Pbp) collisions, resulting in a shift of the effective detector acceptance. In this analysis, $\Upsilon(nS)$ mesons are measured in the kinematic range of $p_{\mathrm{T}} < 25$ GeV/c, and $1.5 < y^* < 4.0$ for pPb forward and $-5.0 < y^* < -2.5$ for pPb backward collisions. This is the first measurement of $\Upsilon(3S)$ production in pPb collisions in this kinematic range. The data samples correspond to an integrated luminosity of $12.5 \pm 0.3\,\mathrm{nb}^{-1}$ in the forward configuration and $19.3 \pm 0.5\,\mathrm{nb}^{-1}$ in the backward

JHEP11(2018)194

configuration. The luminosities are determined using van der Meer scans [47], which were performed for both beam configurations.

3 Definition of the observables

The observables are measured in bins of p_{T} and y^* of the $\Upsilon(1S)$ and $\Upsilon(2S)$ mesons, where both p_{T} and y^* are defined with respect to the direction of the proton beam in the centre-of-mass frame. For the $\Upsilon(3S)$ meson, due to the limited signal yield, only integrated observables are measured.

The differential cross-section is measured in a fixed bin size of 0.5 units for y^* and variable bin sizes for p_{T} in the 0–25 GeV/c range. The $\Upsilon(nS)$ meson double-differential production cross-section in the proton-lead collisions is defined as

$$\frac{\mathrm{d}^2\sigma}{\mathrm{d}p_{\mathrm{T}}\mathrm{d}y^*} = \frac{N(\Upsilon(nS) \to \mu^+\mu^-)}{\mathcal{L} \times \varepsilon_{\mathrm{tot}}^{\Upsilon(nS)} \times \mathcal{B}_{\mu\mu}^{\Upsilon(nS)} \times \Delta p_{\mathrm{T}} \times \Delta y^*}, \tag{3.1}$$

where $N(\Upsilon(nS) \to \mu^+\mu^-)$ is the raw yield of the $\Upsilon(nS)$ decays reconstructed in the given rapidity and transverse momentum bin, $\varepsilon_{\mathrm{tot}}^{\Upsilon(nS)}$ is the total efficiency in that bin, including acceptance, $\mathcal{B}_{\mu\mu}^{\Upsilon(nS)}$ is the branching fraction of the $\Upsilon(nS)$ state to the $\mu^+\mu^-$ final state, and $\mathcal{L}$ is the integrated luminosity of the data sample. The values of the branching fractions used in this measurement are $(2.48 \pm 0.05)\%$ for $\Upsilon(1S) \to \mu^+\mu^-$, $(1.93 \pm 0.17)\%$ for $\Upsilon(2S) \to \mu^+\mu^-$, and $(2.18 \pm 0.21)\%$ for $\Upsilon(3S) \to \mu^+\mu^-$ [48].

The nuclear modification factor for ^{208}Pb is defined for the pPb and Pbp configurations as

$$R_{p\mathrm{Pb}}(p_{\mathrm{T}}, y^*) = \frac{1}{208} \frac{\mathrm{d}^2\sigma_{p\mathrm{Pb}}(p_{\mathrm{T}}, y^*)/\mathrm{d}p_{\mathrm{T}}\mathrm{d}y^*}{\mathrm{d}^2\sigma_{pp}(p_{\mathrm{T}}, y^*)/\mathrm{d}p_{\mathrm{T}}\mathrm{d}y^*}, \tag{3.2}$$

where σ_{pp} is the reference cross-section from pp collisions interpolated to $\sqrt{s} = 8.16$ TeV using the LHCb measurements at $\sqrt{s}$ =2.76, 7, 8, and 13 TeV.

The forward-to-backward ratio is defined as

$$R_{\mathrm{FB}}(p_{\mathrm{T}}, |y^*|) = \frac{\mathrm{d}^2\sigma_{p\mathrm{Pb}}(p_{\mathrm{T}}, +|y^*|)/\mathrm{d}p_{\mathrm{T}}\mathrm{d}y^*}{\mathrm{d}^2\sigma_{\mathrm{Pb}p}(p_{\mathrm{T}}, -|y^*|)/\mathrm{d}p_{\mathrm{T}}\mathrm{d}y^*}, \tag{3.3}$$

and is evaluated in the rapidity range of $2.5 < |y^*| < 4.0$, which is common to pPb and Pbp collisions.

The ratio of excited $\Upsilon(2S)$ and $\Upsilon(3S)$ states to the $\Upsilon(1S)$ ground state in proton-lead collisions is defined as

$$R(\Upsilon(nS)) = \frac{\left[\mathrm{d}^2\sigma/\mathrm{d}p_{\mathrm{T}}dy^*\right](\Upsilon(nS))}{\left[\mathrm{d}^2\sigma/\mathrm{d}p_{\mathrm{T}}dy^*\right](\Upsilon(1S))}. \tag{3.4}$$

In addition, the ratio of $\Upsilon(1S)$ to non-prompt J/ψ cross-sections in proton-lead collisions is measured in the same way. The double ratio

$$\mathfrak{R}^{\Upsilon(nS)/\Upsilon(1S)}_{(p\mathrm{Pb}|\mathrm{Pb}p)/pp} = \frac{R(\Upsilon(nS))_{p\mathrm{Pb}|\mathrm{Pb}p}}{R(\Upsilon(nS))_{pp}} \tag{3.5}$$

compares the ratio $R(\Upsilon(nS))$ in pPb or Pbp collisions to $R(\Upsilon(nS))$ in pp collisions.

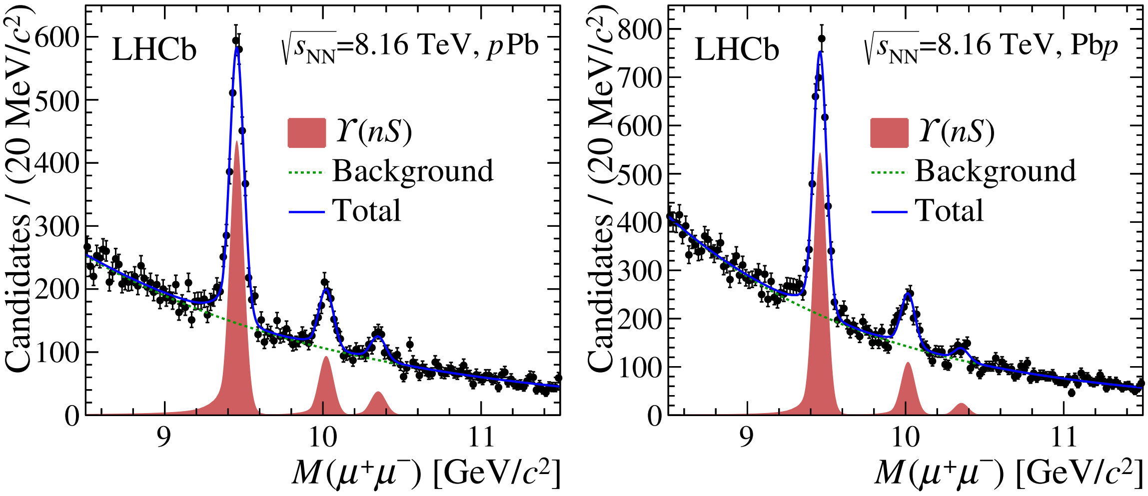

Figure 1. Invariant-mass distribution of $\mu^+\mu^-$ pairs from the (left) pPb and (right) Pbp samples after the trigger and offline selections.

Samples	$\Upsilon(1S)$	$\Upsilon(2S)$	$\Upsilon(3S)$	$\mathcal{L}$
pPb	2705 ± 87	584 ± 49	262 ± 44	$12.5\,\text{nb}^{-1}$
Pbp	3072 ± 82	679 ± 54	159 ± 39	$19.3\,\text{nb}^{-1}$

Table 1. Yields of $\Upsilon(1S)$, $\Upsilon(2S)$, $\Upsilon(3S)$ mesons in pPb and Pbp samples as given by the fit. The uncertainties are statistical only.

4 Event selection

The candidates reconstructed in the trigger are further filtered by means of an offline selection. In the offline selection, there must be at least one PV reconstructed and each PV must have at least four tracks measured in the vertex detector. For events with multiple PVs, the PV that has the smallest $\chi^2_{\rm IP}$ with respect to the $\Upsilon(nS)$ candidate is chosen. Here, $\chi^2_{\rm IP}$ is defined as the difference between the vertex-fit χ^2 calculated with the $\Upsilon(nS)$ meson candidate included in or excluded from the PV fit. Each muon track is required to have $p_{\rm T} > 1\,\text{GeV}/c$, to be in the geometrical acceptance of the spectrometer ($2.0 < \eta < 5.0$), to satisfy PID requirements, and to have a good track-fit quality. The dimuon invariant-mass distribution of offline-selected candidates is shown in figure 1 for the pPb and Pbp samples.

The dimuon invariant-mass distribution is fitted with an exponential function for the background and three separate peaking functions, each consisting of the sum of two Crystal Ball functions [49] for the $\Upsilon(nS)$ peaks. The shape parameters of the double Crystal Ball functions (n and α) are fixed to the values obtained in the simulation. The yields of $\Upsilon(1S)$, $\Upsilon(2S)$, $\Upsilon(3S)$ mesons in the pPb and Pbp samples are summarised in table 1. The probability that the background can produce a fluctuation greater than or equal to the excess observed in data is calculated as the local p-value. For the exponential-background-only fits in the range of $\pm 100\,\text{MeV}/c^2$ around the expected $\Upsilon(3S)$ mass peak, the local p-values are below 10^{-13} in pPb sample and below 10^{-7} in Pbp sample.

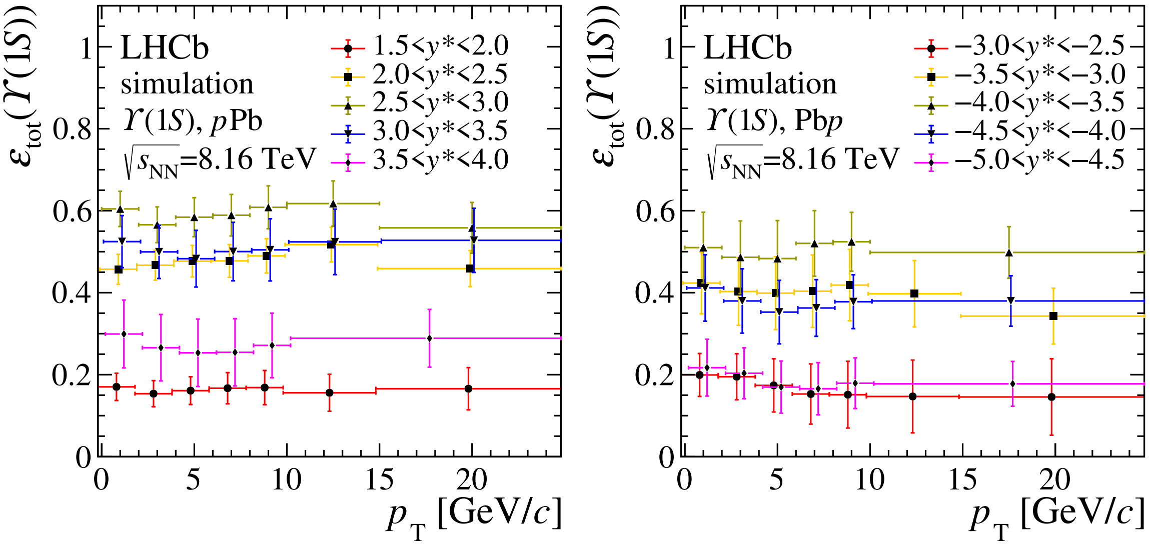

Figure 2. Total efficiency $\varepsilon_{\rm tot}$ of the $\Upsilon(1S)$ meson as a function of its $p_{\rm T}$ in different y^* bins in (left) pPb and (right) Pbp collisions. The horizontal locations of the markers are roughly the centroids of the bins, with offsets from centre to aid in readability.

5 Efficiencies

The signal yields are corrected bin-by-bin by the total efficiencies to obtain the cross-section measurements. The total efficiency $\varepsilon_{\rm tot}$ includes contributions from the geometrical acceptance, the tracking and trigger efficiencies, and the efficiency of the selection including the requirement on the PID of the muons. All efficiencies are determined from simulation apart from the tracking and particle-identification efficiencies, where data are used to correct the efficiencies obtained from the simulation. The same procedure is used for each of the three $\Upsilon(nS)$ states.

The muon tracking efficiency is calculated using simulated $\Upsilon(nS)$ events in pPb and Pbp collisions, and the efficiency in simulation is calibrated using efficiencies estimated from J/ψ candidates selected in pPb data using a tag-and-probe method similar to that adopted in the measurement of J/ψ production using the same data set [29].

The PID efficiency for muons is measured using statistically independent samples of J/ψ decays in pPb, Pbp and pp data. In regions where the number of J/ψ decays is small, the efficiency is determined using weighted data from pp collisions to reproduce the kinematics and detector occupancies of pPb collisions.

The total efficiency for the $\Upsilon(1S)$ state is shown in figure 2. The efficiencies for the $\Upsilon(2S)$ and $\Upsilon(3S)$ states are similar. The uncertainties shown are statistical, due to the limited size of the simulated samples, and systematic, which will be discussed in the next section. The difference in efficiencies as a function of rapidity is largely due to acceptance effects.

Source	pPb	Pbp
Signal detemination	5.7%	5.7%
Acceptance	0.7%–3.4%	0.5%–3.5%
Reconstruction efficiency	2.1%–7.9%	2.5%–8.1%
Offline selection efficiency	0.1%–0.8%	0.1%–1.4%
PID efficiency	1.1%–4.4%	1.9%–6.0%
Trigger efficiency	2.0%–2.8%	2.0%–2.4%
Luminosity	2.6%	2.5%
Branching ratio	2.0%–9.6%	2.0%–9.6%

Table 2. Systematic uncertainties (in percent) on the cross-section measurements. The ranges indicate the minimum and maximum values in different bins, among all $\Upsilon(nS)$ states.

6 Systematic uncertainties

Table 2 summarises the systematic uncertainties, which are different for each of the $\Upsilon(nS)$ states. The finite size of the simulation samples leads to an uncertainty on the efficiency estimation, which is uncorrelated among bins and $\Upsilon(nS)$ states and contributes to the uncertainties in acceptance, offline selection and trigger efficiencies. These uncertainties are small compared to the other systematic uncertainties and barely affect the overall systematic uncertainty. All other uncertainties are correlated among bins.

The choice of the fit model for the mass distributions affects the signal yields. The uncertainty associated with the choice of the fit functions is estimated using different functions (single Crystal Ball functions for signal, and a second-order polynomial for background), and by modifying the fit range for the signal fit to account for the uncertainty due to the radiative tail. The uncertainty due to the choice of the fit models is estimated to be 5.7%.

The track reconstruction efficiency calibration has uncertainties from three sources: the size of the calibration samples, the selection efficiency, and the signal yield determination of the calibration data sample. Considering all these effects, the total uncertainty from the reconstruction of the tracks varies from 2.1% to 7.9% for the pPb sample and from 2.5% to 8.1% for the Pbp sample.

The uncertainty on the offline selection efficiency is only due to the finite size of the simulation sample, varying from 0.1% to 1.4%.

The PID uncertainties are related to the limited size of the pp and pPb (Pbp) calibration samples, and to the difference between the pp and pPb (Pbp) PID calibration samples. The latter effects lead to an uncertainty on the PID efficiency varying from 1.1% to 3.9% for the pPb sample and from 1.9% to 2.8% for the Pbp sample. The total PID uncertainty including all effects varies from 1.1% to 4.4% for the pPb sample and from 1.9% to 6.0% for the Pbp sample.

The trigger efficiency is obtained from simulation. The limited size of the simulated samples contributes to kinematic-bin-dependent uncertainties that vary between 0.2% and 2.0% for the pPb sample and between 0.2% and 1.2% in the Pbp sample. An additional uncertainty of 2.0% is assigned based on a study of the trigger efficiency on a calibration data sample.

The relative uncertainty on the pPb luminosity determined by the van der Meer scan is 2.6% and that on the Pbp luminosity is 2.5%.

The uncertainties from the decay branching fractions of the $\Upsilon(nS)$ states contribute to the systematic uncertainty for values between 2.0 and 9.6%[48].

7 Results

The total $\Upsilon(nS)$ cross-sections in the kinematic region $p_{\mathrm{T}} < 25\,\mathrm{GeV/c}$ and $1.5 < y^* < 4.0$ ($-5.0 < y^* < -2.5$) for pPb (Pbp) sample are measured to be

$$\begin{aligned}
\sigma^{\Upsilon(1S)}_{p\mathrm{Pb}} &= 22.8 \pm 0.9\ (\mathrm{stat}) \pm 2.1\ (\mathrm{syst})\ \mu\mathrm{b},\\
\sigma^{\Upsilon(2S)}_{p\mathrm{Pb}} &= 6.4 \pm 0.6\ (\mathrm{stat}) \pm 0.8\ (\mathrm{syst})\ \mu\mathrm{b},\\
\sigma^{\Upsilon(3S)}_{p\mathrm{Pb}} &= 2.5 \pm 0.4\ (\mathrm{stat}) \pm 0.3\ (\mathrm{syst})\ \mu\mathrm{b},\\
\sigma^{\Upsilon(1S)}_{\mathrm{Pb}p} &= 20.3 \pm 0.8\ (\mathrm{stat}) \pm 2.6\ (\mathrm{syst})\ \mu\mathrm{b},\\
\sigma^{\Upsilon(2S)}_{\mathrm{Pb}p} &= 6.0 \pm 0.5\ (\mathrm{stat}) \pm 0.9\ (\mathrm{syst})\ \mu\mathrm{b},\\
\sigma^{\Upsilon(3S)}_{\mathrm{Pb}p} &= 1.2 \pm 0.3\ (\mathrm{stat}) \pm 0.2\ (\mathrm{syst})\ \mu\mathrm{b}.
\end{aligned}$$

The cross-sections are also evaluated as a function of p_{T} and y^* for the $\Upsilon(1S)$ and $\Upsilon(2S)$ states. The double-differential cross-section for the $\Upsilon(1S)$ state is shown in figure 3. It is integrated over p_{T} to form a differential cross-section as a function of y^*, as shown in figure 4 (left), and integrated over y^* to form a differential cross-section as a function of p_{T}, as shown in figure 5 (left).[1] Similarly, for the $\Upsilon(2S)$ state the differential cross-section as a function of y^* and p_{T} are shown in figure 4 (right) and figure 5 (right), respectively. For the $\Upsilon(3S)$ state, due to the limited sample size, only the cross-section integrated over p_{T} and y^* is measured.

To measure the nuclear modification factor, a measurement of the pp cross-section at the same centre-of-mass energy is needed. In the absence of a direct measurement, the value of the $\Upsilon(nS)$ cross-section in pp collisions at $\sqrt{s} = 8.16$ TeV is obtained by interpolating between the values measured in pp collisions by LHCb at 2.76, 7, 8 and 13 TeV [50–52] using a second-order polynomial function. The differences between the scale factors obtained using the nominal second-order polynomial fits and alternative fits using exponential functions are assigned as systematic uncertainties on the interpolated cross-sections. The values of the $\Upsilon(1S)$ and $\Upsilon(2S)$ differential cross-sections in p_{T} (y^*) integrated over y^* (p_{T}) in pp collisions at $\sqrt{s} = 8.16\,\mathrm{TeV}$ are shown in figures 4 to 5, and their numerical values are provided in appendix B. The production of both $\Upsilon(1S)$ and $\Upsilon(2S)$ is suppressed in the forward pPb region with respect to the scaled value from pp collisions, as already observed in the prompt J/ψ measurement [29], while no significant suppression is visible in the backward Pbp region. The nuclear modification factors are

---

[1] The numerical results of all cross-section measurements shown in this section can be found in appendix A.

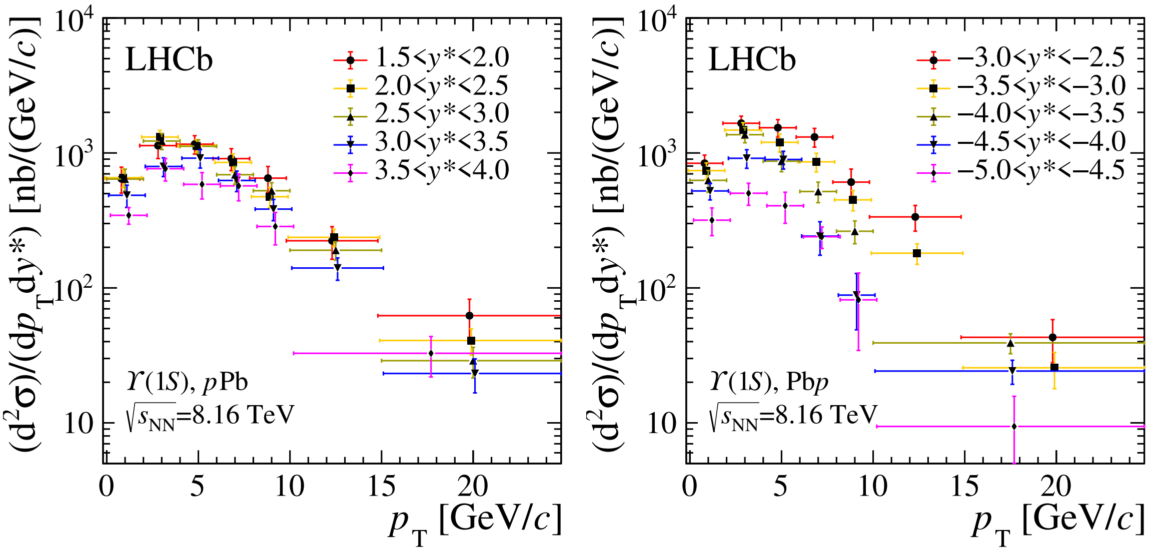

Figure 3. Double-differential cross-section for the $\Upsilon(1S)$ meson as a function of p_{T} for different values of y^* for the (left) forward pPb and (right) backward Pbp samples. The uncertainties are the sums in quadrature of the statistical and systematic components. The horizontal locations of the markers are roughly the centroids of the bins, with offsets from centre to aid in readability.

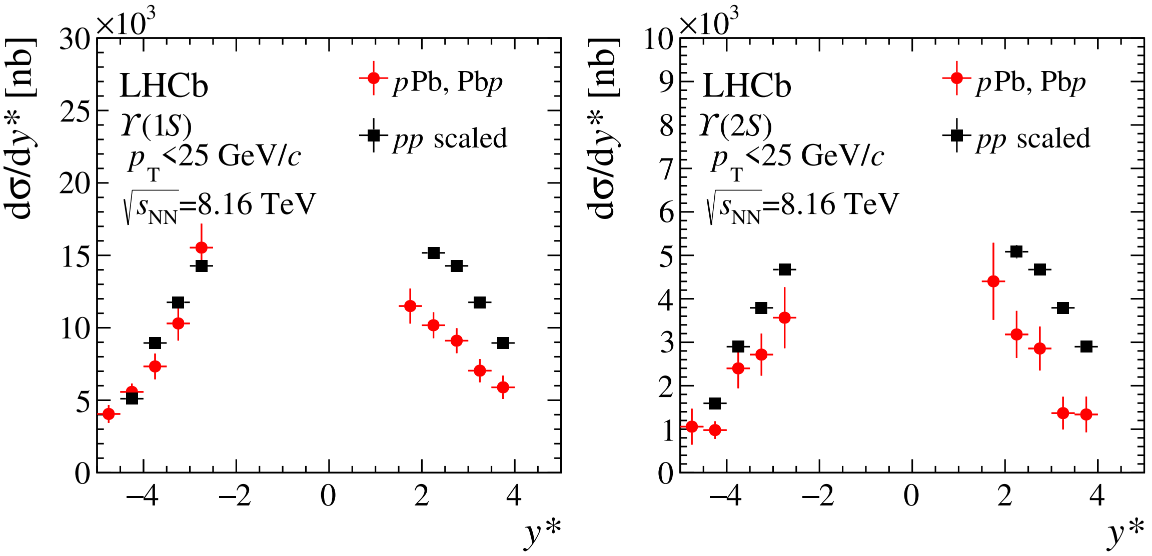

Figure 4. Cross-section of (left) $\Upsilon(1S)$ and (right) $\Upsilon(2S)$ production as a function of y^* integrated over p_{T} for the backward (negative y^*) and forward (positive y^*) samples, compared to the cross-section measured in pp, interpolated to $\sqrt{s_{\mathrm{NN}}} = 8.16\,\mathrm{TeV}$. In this and subsequent figures, the uncertainties shown are the sums in quadrature of the statistical and systematic components.

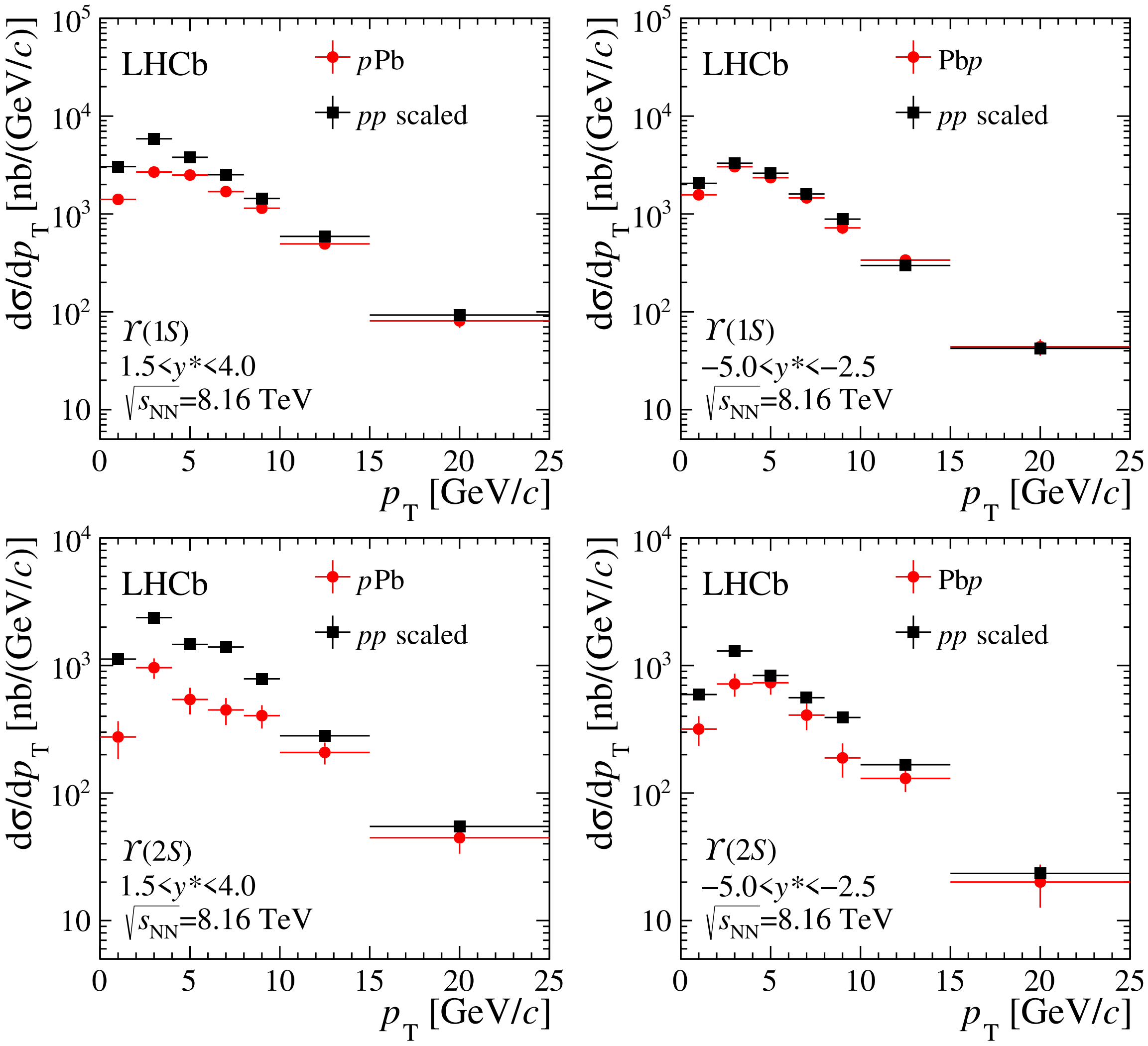

Figure 5. Cross-section of (top) $\Upsilon(1S)$ and (bottom) $\Upsilon(2S)$ production as a function of p_{T} integrated over y^* for the (left) forward and (right) backward samples compared to the cross-section measured in pp, interpolated to $\sqrt{s_{\mathrm{NN}}} = 8.16$ TeV.

evaluated as functions of p_{T} and y^* for the $\Upsilon(1S)$ and $\Upsilon(2S)$ states,[2] and compared with different theoretical calculations:

1. A calculation based on the "HELAC-Onia" framework [53–55], where the modification of the parton flux due to CNM is treated within the collinear factorisation framework using two different nuclear parton distribution functions (nPDFs), the EPPS16 [56] and nCTEQ15 nPDFs set [7].

2. Calculations based on the *comovers* model of $\Upsilon(nS)$ production [17, 18], which implements final state interaction of the quarkonia states and nuclear parton distribution function modification via EPS09 at leading order [6], and the nCTEQ15 set already described.

---

[2] In the nuclear modification factors, the systematic uncertainty related to branching ratios cancels.

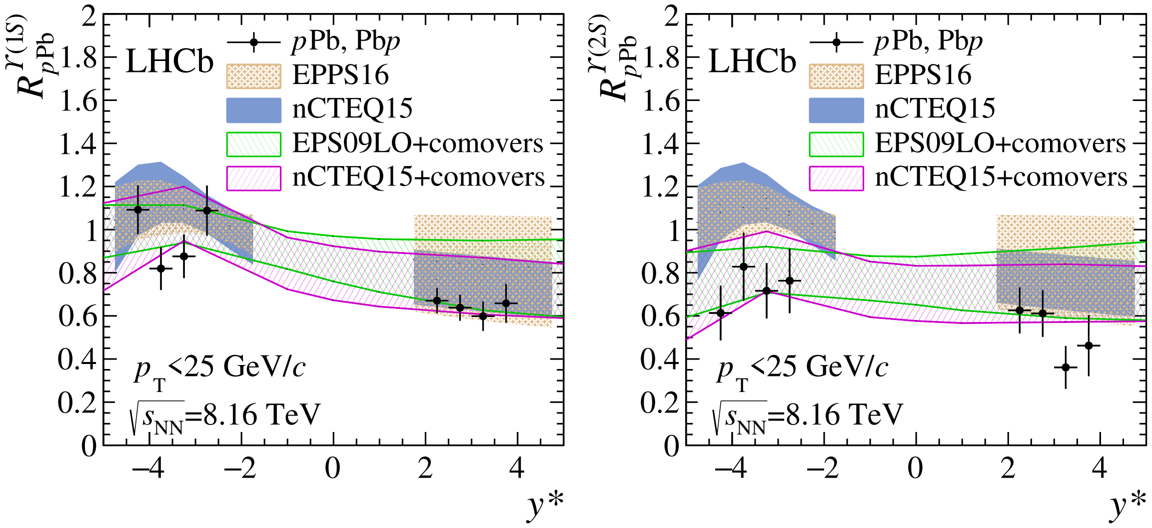

Figure 6. Nuclear modification factors of the (left) $\Upsilon(1S)$ and (right) $\Upsilon(2S)$ mesons as a function of y^* integrated over p_{T} for the forward and backward samples. The bands correspond to the theoretical predictions for the nCTEQ15 and EPPS16 nPDFs sets, and the comovers model as reported in the text.

The measurements and the calculations are shown in figures 6 and 7. For the $\Upsilon(1S)$ state the nuclear modification factor is about 0.5 (0.8) at low p_{T} in the forward (backward) region, and is consistent with unity for p_{T} larger than 10 GeV/c, as predicted by the models. As a function of rapidity, $R_{p\mathrm{Pb}}$ is consistent with unity in the Pbp region at negative $|y^*|$, while a suppression is observed in the pPb region, where it averages around 0.7, consistent with the models analysed. The nuclear modification factor for $\Upsilon(2S)$ is smaller than $\Upsilon(1S)$, which is consistent with the comovers models. The corresponding numerical results can be found in appendix C. The same trend as for the $\Upsilon(1S)$ state is observed for the $\Upsilon(2S)$state, although the suppression seems more pronounced for the $\Upsilon(2S)$ state, as already observed by other experiments [22], especially in the backward region.

The forward-backward asymmetry is evaluated only for the $\Upsilon(1S)$ meson as a function of p_{T} and y^*, see figure 8, whereas for the $\Upsilon(2S)$ meson it is integrated over both y^* and p_{T} as shown in figure 9. The corresponding numerical results can be found in appendix D.[3]

The ratio of the cross-sections of $\Upsilon(2S)$ and $\Upsilon(1S)$ mesons as a function of p_{T}, integrated over y^*, and as function of y^*, integrated over p_{T}, are shown in figure 10. The corresponding numerical results can be found in appendix E. The ratios confirmed a larger suppression for the excited states with respect to the ground state observed in proton-lead collisions compared to pp collisions [51]. For the $\Upsilon(3S)$ state, due to the limited size of the data sample, only an integral ratio is measured. In the determination of the ratio $R(\Upsilon(nS))$, most of the systematic uncertainties cancel, except that related to branching ratios.

The integrated ratios are summarised in table 3, where values are also reported for pp collisions. The corresponding double-ratio results are shown in figure 11 (left), together

---

[3] In the forward-backward ratio, the systematic uncertainty related to branching ratios cancels.

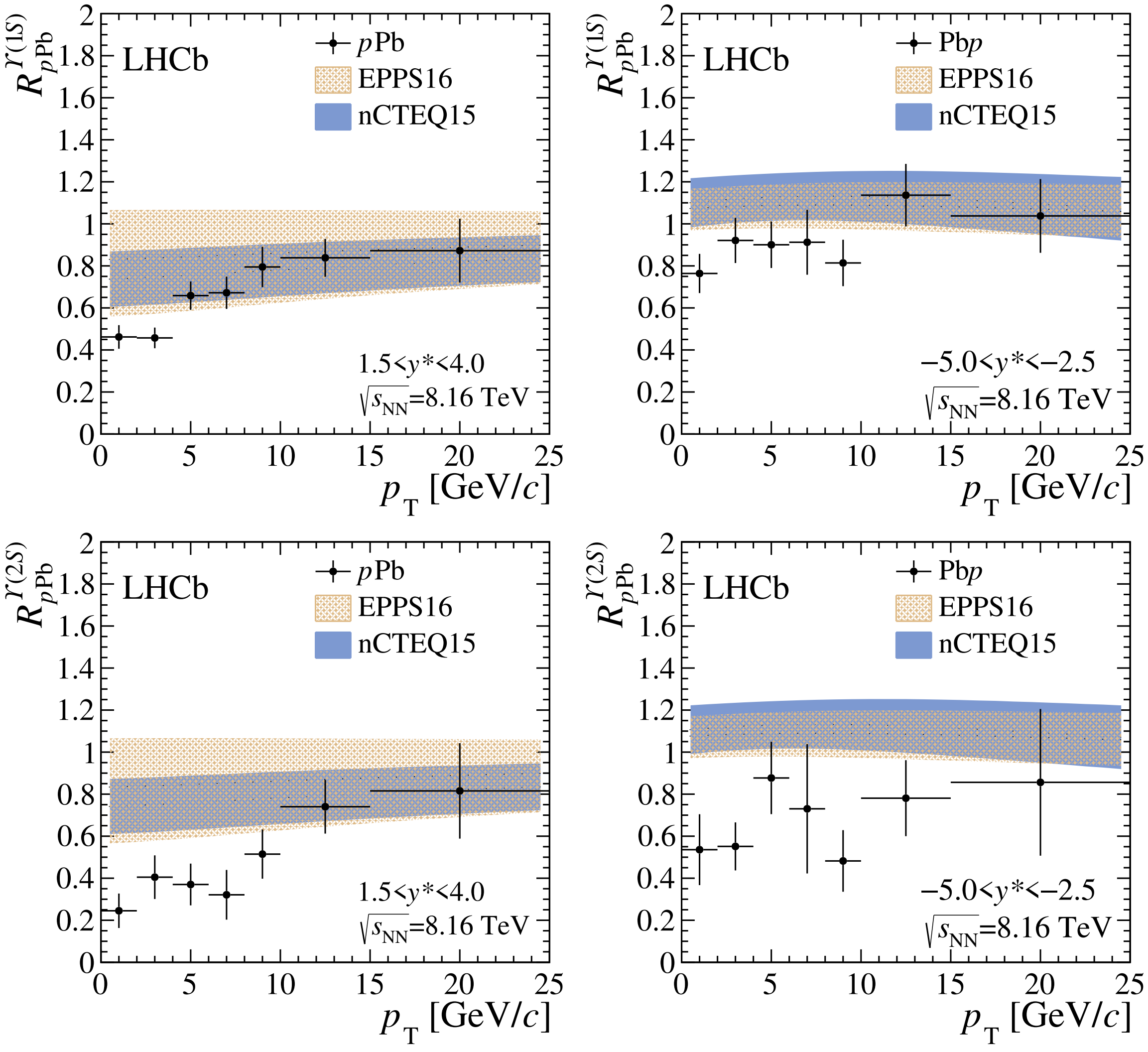

Figure 7. Nuclear modification factors of the (top) $\Upsilon(1S)$ and (bottom) $\Upsilon(2S)$ mesons as a function of p_{T} integrated over y^* for the (left) forward and (right) backward samples. The bands correspond to the theoretical predictions for the nCTEQ15 and EPPS16 nPDFs sets as reported in the text.

with the comovers model calculations, and the numerical results are

$$\mathfrak{R}_{p\mathrm{Pb}/pp}^{\Upsilon(2S)/\Upsilon(1S)} = 0.86 \pm 0.15,$$
$$\mathfrak{R}_{p\mathrm{Pb}/pp}^{\Upsilon(3S)/\Upsilon(1S)} = 0.81 \pm 0.15,$$
$$\mathfrak{R}_{\mathrm{Pb}p/pp}^{\Upsilon(2S)/\Upsilon(1S)} = 0.91 \pm 0.21,$$
$$\mathfrak{R}_{\mathrm{Pb}p/pp}^{\Upsilon(3S)/\Upsilon(1S)} = 0.44 \pm 0.15.$$

For the double ratio of the $\Upsilon(3S)$ over $\Upsilon(1S)$ in the backward a clear indication of stronger suppression is observed, in agreement with the comovers model as shown in figure 11 (right). The ratio of the $\Upsilon(1S)$ and nonprompt J/ψ cross-sections in pPb and Pbp collisions is also measured, where the nonprompt J/ψ cross-section was measured previously by LHCb [29]

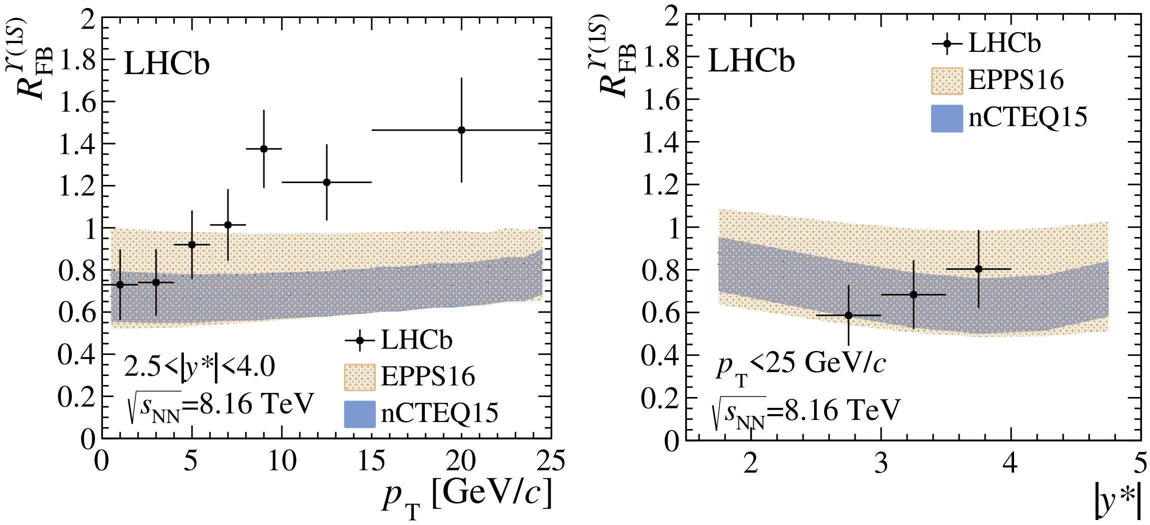

Figure 8. Forward-backward ratio for the $\Upsilon(1S)$ as a function of (left) p_{T} integrated over y^* and (right) as a function of $|y^*|$ integrated over p_{T}. The bands correspond to the theoretical calculations for the nCTEQ15 and EPPS16 nPDFs sets as reported in the text.

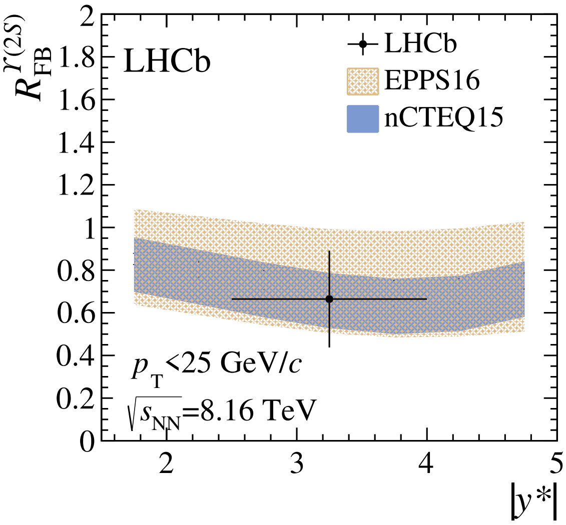

Figure 9. Forward-backward ratio for the $\Upsilon(2S)$ compared with theoretical calculations for the nCTEQ15 and EPPS16 nPDFs sets as reported in the text.

using the same data sample. The ratio is shown in figure 12 compared to the corresponding result observed in pp collisions. The numerical results are reported in appendix F. A small suppression is visible, which could be attributed to final-state CNM effects. More data are needed in order to have a more definite indication of a different suppression mechanism for bottomonium and open beauty, such as $\Upsilon(1S)$ and nonprompt J/ψ states, as indicated by refs. [57, 58].

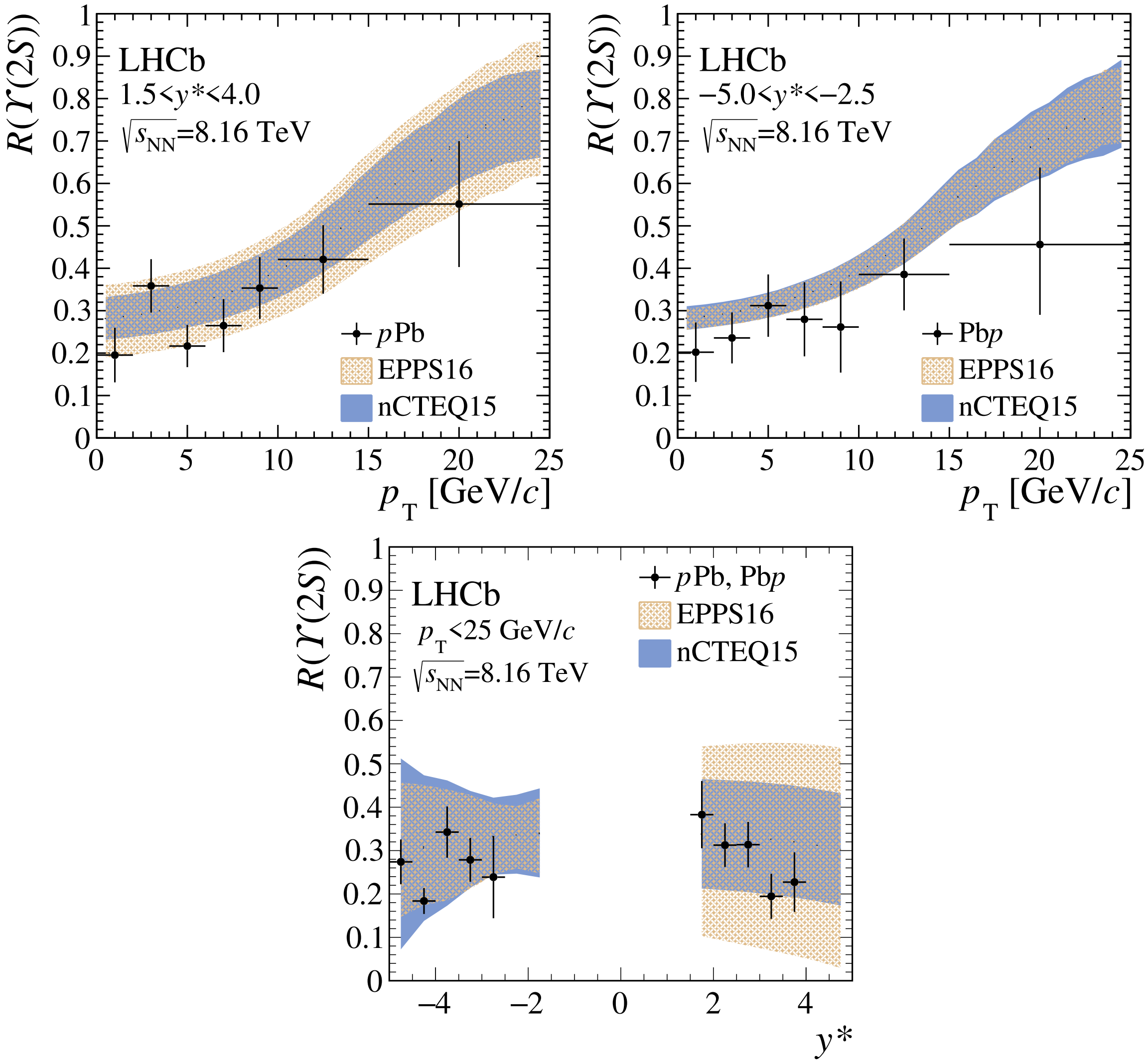

Figure 10. Ratios between $\Upsilon(2S)$ and $\Upsilon(1S)$ cross-sections as a function of (top) p_{T} integrated over y^*, and as function of (bottom) y^* integrated over p_{T}, for pPb and Pbp collisions. The bands correspond to the theoretical predictions for the nCTEQ15 and EPPS16 nPDFs sets as reported in the text.

Sample		$R(\Upsilon(2S))$	$R(\Upsilon(3S))$
pp	$2.0 < y^* < 4.0$	0.328 ± 0.004	0.137 ± 0.002
pp	$-4.5 < y^* < -2.5$	0.325 ± 0.004	0.137 ± 0.002
pPb	$2.0 < y^* < 4.0$	0.282 ± 0.050	0.11 ± 0.02
Pbp	$-4.5 < y^* < -2.5$	0.296 ± 0.070	0.06 ± 0.02

Table 3. Ratio $R(\Upsilon(nS))$ in pp, pPb, and Pbp samples. The uncertainties are combinations of statistical and systematical components.

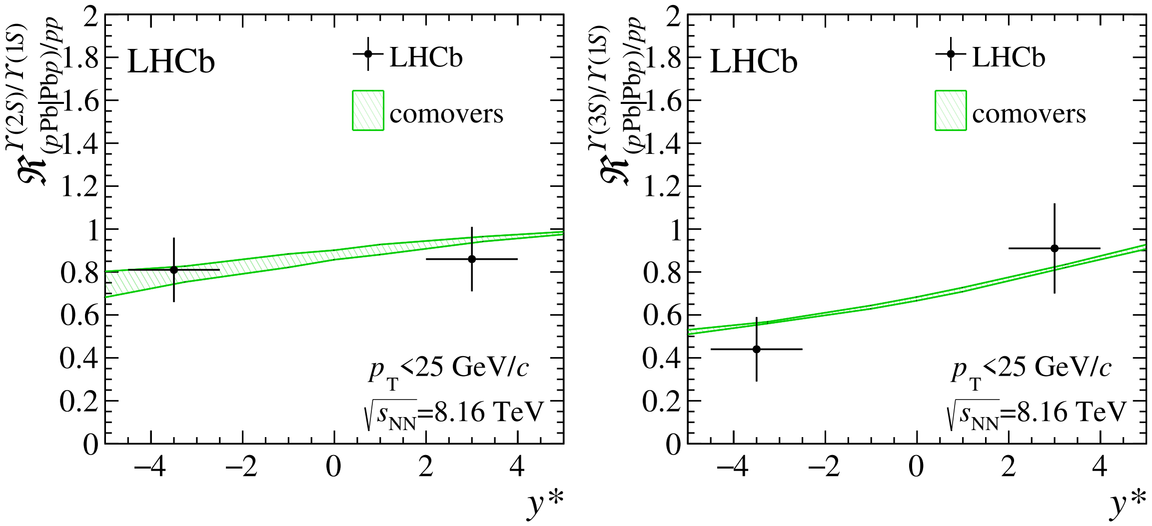

Figure 11. Double ratios for (left) $\Upsilon(2S)$ and (right) $\Upsilon(3S)$. The bands correspond to the theoretical prediction for the comovers model as reported in the text.

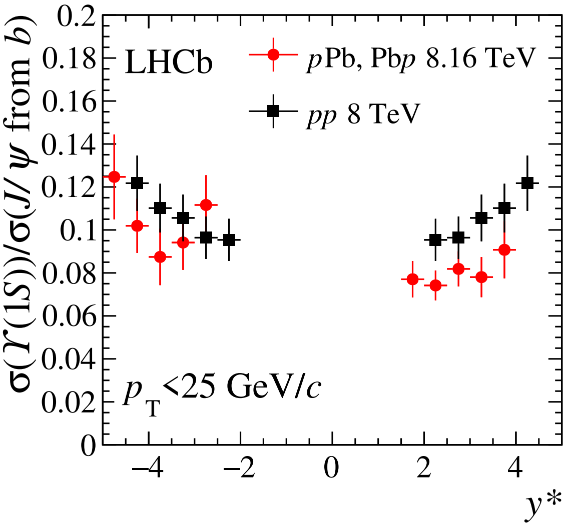

Figure 12. Ratio of $\Upsilon(1S)$ to nonprompt J/ψ cross-sections as a function of y^* integrated over p_T, for pPb and Pbp collisions.

8 Summary

The production of $\Upsilon(nS)$ states is studied in proton-lead collisions at $\sqrt{s_{NN}} = 8.16$ TeV using data collected by the LHCb detector in 2016. The cross-sections, nuclear modification factors and forward-backward ratios are measured double-differentially ($\Upsilon(1S)$) and single-differentially ($\Upsilon(2S)$). The ratios of the production cross-sections of the different $\Upsilon(nS)$ states are also measured as functions of transverse momentum and rapidity in the nucleon-nucleon centre-of-mass frame. The results are consistent with previous observations and with the theoretical model calculations, indicating a suppression of $\Upsilon(nS)$ production in proton-lead collisions up to about 40%, more pronounced for the excited Υ states, particularly in the region of negative rapidity.

Acknowledgments

We thank the theorists who provided predictions for our measurements: J.-P. Lansberg, H.-S. Shao and E. Gonzalez-Ferreiro. We express our gratitude to our colleagues in the CERN accelerator departments for the excellent performance of the LHC. We thank the technical and administrative staff at the LHCb institutes. We acknowledge support from CERN and from the national agencies: CAPES, CNPq, FAPERJ and FINEP (Brazil); MOST and NSFC (China); CNRS/IN2P3 (France); BMBF, DFG and MPG (Germany); INFN (Italy); NWO (Netherlands); MNiSW and NCN (Poland); MEN/IFA (Romania); MSHE (Russia); MinECo (Spain); SNSF and SER (Switzerland); NASU (Ukraine); STFC (United Kingdom); NSF (U.S.A.). We acknowledge the computing resources that are provided by CERN, IN2P3 (France), KIT and DESY (Germany), INFN (Italy), SURF (Netherlands), PIC (Spain), GridPP (United Kingdom), RRCKI and Yandex LLC (Russia), CSCS (Switzerland), IFIN-HH (Romania), CBPF (Brazil), PL-GRID (Poland) and OSC (U.S.A.). We are indebted to the communities behind the multiple open-source software packages on which we depend. Individual groups or members have received support from AvH Foundation (Germany); EPLANET, Marie Skłodowska-Curie Actions and ERC (European Union); ANR, Labex P2IO and OCEVU, and Région Auvergne-Rhône-Alpes (France); Key Research Program of Frontier Sciences of CAS, CAS PIFI, and the Thousand Talents Program (China); RFBR, RSF and Yandex LLC (Russia); GVA, XuntaGal and GENCAT (Spain); the Royal Society and the Leverhulme Trust (United Kingdom); Laboratory Directed Research and Development program of LANL (U.S.A.).

A Cross-section

Tables 4 and 5 list the double-differential cross-section for $\Upsilon(1S)$ in pPb forward and backward samples. Tables 6 and 7 list the differential cross-section for $\Upsilon(1S)$ in bins of transverse momentum and rapidity. The corresponding values for the $\Upsilon(2S)$ state are listed in tables 8 and 9. In all tables, the quoted uncertainties are the sum in quadrature of the statistical and systematic components.

p_{T} [GeV/c]	y^*	$\frac{\mathrm{d}^2\sigma}{\mathrm{d}p_{\mathrm{T}}\mathrm{d}y^*}$ [nb/(GeV/c)]
$0<p_{\mathrm{T}}<2$	$1.5<y^*<2.0$	644 ± 142
$0<p_{\mathrm{T}}<2$	$2.0<y^*<2.5$	656 ± 106
$0<p_{\mathrm{T}}<2$	$2.5<y^*<3.0$	641 ± 119
$0<p_{\mathrm{T}}<2$	$3.0<y^*<3.5$	486 ± 92
$0<p_{\mathrm{T}}<2$	$3.5<y^*<4.0$	345 ± 50
$2<p_{\mathrm{T}}<4$	$1.5<y^*<2.0$	1134 ± 227
$2<p_{\mathrm{T}}<4$	$2.0<y^*<2.5$	1312 ± 163
$2<p_{\mathrm{T}}<4$	$2.5<y^*<3.0$	1226 ± 171
$2<p_{\mathrm{T}}<4$	$3.0<y^*<3.5$	794 ± 129
$2<p_{\mathrm{T}}<4$	$3.5<y^*<4.0$	765 ± 147
$4<p_{\mathrm{T}}<6$	$1.5<y^*<2.0$	1162 ± 184
$4<p_{\mathrm{T}}<6$	$2.0<y^*<2.5$	1130 ± 128
$4<p_{\mathrm{T}}<6$	$2.5<y^*<3.0$	1121 ± 135
$4<p_{\mathrm{T}}<6$	$3.0<y^*<3.5$	915 ± 147
$4<p_{\mathrm{T}}<6$	$3.5<y^*<4.0$	586 ± 132
$6<p_{\mathrm{T}}<8$	$1.5<y^*<2.0$	908 ± 171
$6<p_{\mathrm{T}}<8$	$2.0<y^*<2.5$	851 ± 135
$6<p_{\mathrm{T}}<8$	$2.5<y^*<3.0$	690 ± 106
$6<p_{\mathrm{T}}<8$	$3.0<y^*<3.5$	625 ± 111
$6<p_{\mathrm{T}}<8$	$3.5<y^*<4.0$	570 ± 131
$8<p_{\mathrm{T}}<10$	$1.5<y^*<2.0$	651 ± 145
$8<p_{\mathrm{T}}<10$	$2.0<y^*<2.5$	474 ± 83
$8<p_{\mathrm{T}}<10$	$2.5<y^*<3.0$	525 ± 79
$8<p_{\mathrm{T}}<10$	$3.0<y^*<3.5$	384 ± 71
$8<p_{\mathrm{T}}<10$	$3.5<y^*<4.0$	285 ± 79
$10<p_{\mathrm{T}}<15$	$1.5<y^*<2.0$	224 ± 61
$10<p_{\mathrm{T}}<15$	$2.0<y^*<2.5$	237 ± 36
$10<p_{\mathrm{T}}<15$	$2.5<y^*<3.0$	190 ± 30
$10<p_{\mathrm{T}}<15$	$3.0<y^*<3.5$	140 ± 28
$10<p_{\mathrm{T}}<25$	$3.5<y^*<4.0$	33 ± 11
$15<p_{\mathrm{T}}<25$	$1.5<y^*<2.0$	62 ± 20
$15<p_{\mathrm{T}}<25$	$2.0<y^*<2.5$	41 ± 9
$15<p_{\mathrm{T}}<25$	$2.5<y^*<3.0$	29 ± 8
$15<p_{\mathrm{T}}<25$	$3.0<y^*<3.5$	23 ± 7

Table 4. $\Upsilon(1S)$ production cross-section in pPb, as a function of p_{T} and y^*.

p_{T} [GeV/c]	y^*	$\frac{\mathrm{d}^2\sigma}{\mathrm{d}p_{\mathrm{T}}\mathrm{d}y^*}$ [nb/(GeV/c)]
$0 < p_{\mathrm{T}} < 2$	$-3.0 < y^* < -2.5$	839 ± 130
$0 < p_{\mathrm{T}} < 2$	$-3.5 < y^* < -3.0$	740 ± 114
$0 < p_{\mathrm{T}} < 2$	$-4.0 < y^* < -3.5$	627 ± 129
$0 < p_{\mathrm{T}} < 2$	$-4.5 < y^* < -4.0$	523 ± 90
$0 < p_{\mathrm{T}} < 2$	$-5.0 < y^* < -4.5$	318 ± 77
$2 < p_{\mathrm{T}} < 4$	$-3.0 < y^* < -2.5$	1661 ± 228
$2 < p_{\mathrm{T}} < 4$	$-3.5 < y^* < -3.0$	1478 ± 225
$2 < p_{\mathrm{T}} < 4$	$-4.0 < y^* < -3.5$	1366 ± 216
$2 < p_{\mathrm{T}} < 4$	$-4.5 < y^* < -4.0$	913 ± 164
$2 < p_{\mathrm{T}} < 4$	$-5.0 < y^* < -4.5$	503 ± 99
$4 < p_{\mathrm{T}} < 6$	$-3.0 < y^* < -2.5$	1538 ± 243
$4 < p_{\mathrm{T}} < 6$	$-3.5 < y^* < -3.0$	1199 ± 204
$4 < p_{\mathrm{T}} < 6$	$-4.0 < y^* < -3.5$	869 ± 165
$4 < p_{\mathrm{T}} < 6$	$-4.5 < y^* < -4.0$	895 ± 152
$4 < p_{\mathrm{T}} < 6$	$-5.0 < y^* < -4.5$	406 ± 107
$6 < p_{\mathrm{T}} < 8$	$-3.0 < y^* < -2.5$	1313 ± 222
$6 < p_{\mathrm{T}} < 8$	$-3.5 < y^* < -3.0$	859 ± 149
$6 < p_{\mathrm{T}} < 8$	$-4.0 < y^* < -3.5$	518 ± 99
$6 < p_{\mathrm{T}} < 8$	$-4.5 < y^* < -4.0$	242 ± 69
$6 < p_{\mathrm{T}} < 8$	$-5.0 < y^* < -4.5$	240 ± 45
$8 < p_{\mathrm{T}} < 10$	$-3.0 < y^* < -2.5$	608 ± 156
$8 < p_{\mathrm{T}} < 10$	$-3.5 < y^* < -3.0$	449 ± 83
$8 < p_{\mathrm{T}} < 10$	$-4.0 < y^* < -3.5$	263 ± 53
$8 < p_{\mathrm{T}} < 10$	$-4.5 < y^* < -4.0$	88 ± 40
$8 < p_{\mathrm{T}} < 10$	$-5.0 < y^* < -4.5$	82 ± 47
$10 < p_{\mathrm{T}} < 15$	$-3.0 < y^* < -2.5$	336 ± 75
$10 < p_{\mathrm{T}} < 15$	$-3.5 < y^* < -3.0$	181 ± 33
$10 < p_{\mathrm{T}} < 25$	$-4.0 < y^* < -3.5$	39 ± 7
$10 < p_{\mathrm{T}} < 25$	$-4.5 < y^* < -4.0$	24 ± 5
$10 < p_{\mathrm{T}} < 25$	$-5.0 < y^* < -4.5$	9 ± 6
$15 < p_{\mathrm{T}} < 25$	$-3.0 < y^* < -2.5$	43 ± 15
$15 < p_{\mathrm{T}} < 25$	$-3.5 < y^* < -3.0$	26 ± 8

Table 5. $\Upsilon(1S)$ production cross-section in Pbp, as a function of p_{T} and y^*.

JHEP11(2018)194

p_{T} (GeV/c)	$\frac{\mathrm{d}\sigma}{\mathrm{d}p_{\mathrm{T}}}$ in pPb [nb/(GeV/c)]	$\frac{\mathrm{d}\sigma}{\mathrm{d}p_{\mathrm{T}}}$ in Pbp [nb/(GeV/c)]
$0 < p_{\mathrm{T}} < 2$	1409 ± 164	1570 ± 234
$2 < p_{\mathrm{T}} < 4$	2683 ± 287	3040 ± 437
$4 < p_{\mathrm{T}} < 6$	2500 ± 268	2349 ± 341
$6 < p_{\mathrm{T}} < 8$	1693 ± 197	1461 ± 203
$8 < p_{\mathrm{T}} < 10$	1145 ± 142	721 ± 107
$10 < p_{\mathrm{T}} < 15$	495 ± 61	338 ± 48
$15 < p_{\mathrm{T}} < 25$	81 ± 13	44 ± 9

Table 6. $\Upsilon(1S)$ production cross-section in pPb and Pbp, as a function of p_{T}.

y^*	$\frac{\mathrm{d}\sigma}{\mathrm{d}y^*}$ [nb]
$-5.0 < y^* < -4.5$	4050 ± 646
$-4.5 < y^* < -4.0$	5572 ± 720
$-4.0 < y^* < -3.5$	7333 ± 1109
$-3.5 < y^* < -3.0$	10300 ± 1399
$-3.0 < y^* < -2.5$	15531 ± 1868
$1.5 < y^* < 2.0$	11500 ± 1266
$2.0 < y^* < 2.5$	10175 ± 955
$2.5 < y^* < 3.0$	9107 ± 908
$3.0 < y^* < 3.5$	7038 ± 843
$3.5 < y^* < 4.0$	5891 ± 862

Table 7. $\Upsilon(1S)$ production cross-section in pPb and Pbp, as a function of y^*.

JHEP11(2018)194

p_{T} [GeV/c]	$\dfrac{\mathrm{d}\sigma}{\mathrm{d}p_{\mathrm{T}}}$ in pPb [nb/(GeV/c)]	$\dfrac{\mathrm{d}\sigma}{\mathrm{d}p_{\mathrm{T}}}$ in Pbp [nb/(GeV/c)]
$0 < p_{\mathrm{T}} < 2$	275 ± 91	317 ± 83
$2 < p_{\mathrm{T}} < 4$	962 ± 179	717 ± 148
$4 < p_{\mathrm{T}} < 6$	542 ± 129	733 ± 142
$6 < p_{\mathrm{T}} < 8$	448 ± 109	409 ± 97
$8 < p_{\mathrm{T}} < 10$	405 ± 86	189 ± 57
$10 < p_{\mathrm{T}} < 15$	208 ± 42	130 ± 28
$15 < p_{\mathrm{T}} < 25$	45 ± 11	20 ± 7

Table 8. $\Upsilon(2S)$ production cross-section in pPb and Pbp, as a function of p_{T}.

y^*	$\dfrac{\mathrm{d}\sigma}{\mathrm{d}y^*}$ [nb]
$-5.0 < y^* < -4.5$	1058 ± 414
$-4.5 < y^* < -4.0$	979 ± 202
$-4.0 < y^* < -3.5$	2400 ± 458
$-3.5 < y^* < -3.0$	2716 ± 485
$-3.0 < y^* < -2.5$	3565 ± 702
$1.5 < y^* < 2.0$	4402 ± 898
$2.0 < y^* < 2.5$	3180 ± 551
$2.5 < y^* < 3.0$	2856 ± 515
$3.0 < y^* < 3.5$	1369 ± 381
$3.5 < y^* < 4.0$	1339 ± 416

Table 9. $\Upsilon(2S)$ production cross-section in pPb, as a function of y^*.

B Scaled $\Upsilon(1S)$ and $\Upsilon(2S)$ differential cross-sections in pp collisions

Tables 10 and 11 show the $\Upsilon(1S)$ and $\Upsilon(2S)$ differential cross-sections scaled to the cross-section in pp collisions at $\sqrt{s_{\mathrm{NN}}} = 8.16\,\mathrm{TeV}$ in p_{T} integrated over y in region $2.0 < y < 4.5$ and in y over p_{T} in region $p_{\mathrm{T}} < 25$ GeV/c.

p_{T} [GeV/c]	$\Upsilon(1S)$ $\frac{\mathrm{d}\sigma}{\mathrm{d}p_{\mathrm{T}}}$ [nb/(GeV/c)]	$\Upsilon(2S)$ $\frac{\mathrm{d}\sigma}{\mathrm{d}p_{\mathrm{T}}}$ [nb/(GeV/c)]
$0 < p_{\mathrm{T}} < 2$	$1995 \pm 14 \pm 31$	$555 \pm 9 \pm 11$
$2 < p_{\mathrm{T}} < 4$	$3626 \pm 18 \pm 51$	$1052 \pm 11 \pm 19$
$4 < p_{\mathrm{T}} < 6$	$2898 \pm 16 \pm 40$	$910 \pm 11 \pm 15$
$6 < p_{\mathrm{T}} < 8$	$1786 \pm 12 \pm 28$	$634 \pm 9 \pm 14$
$8 < p_{\mathrm{T}} < 10$	$1009 \pm 9 \pm 15$	$394 \pm 7 \pm 7$
$10 < p_{\mathrm{T}} < 15$	$382 \pm 5 \pm 7$	$169 \pm 4 \pm 4$
$15 < p_{\mathrm{T}} < 25$	$54 \pm 2 \pm 1$	$29 \pm 1 \pm 1$

Table 10. Scaled pp differential cross-section in p_{T} at $\sqrt{s_{\mathrm{NN}}} = 8.16\,\mathrm{TeV}$. The first uncertainty is statistical, the second is systematic, which includes the systematic uncertainty from the pp measurement and that estimated by changing the interpolation function.

y	$\Upsilon(1S)$ $\frac{\mathrm{d}\sigma}{\mathrm{d}y}$ [nb]	$\Upsilon(2S)$ $\frac{\mathrm{d}\sigma}{\mathrm{d}y}$ [nb]
$2.0 < y < 2.5$	$15171 \pm 143 \pm 250$	$5083 \pm 105 \pm 110$
$2.5 < y < 3.0$	$14273 \pm 82 \pm 193$	$4672 \pm 60 \pm 79$
$3.0 < y < 3.5$	$11758 \pm 66 \pm 170$	$3792 \pm 49 \pm 71$
$3.5 < y < 4.0$	$8950 \pm 65 \pm 137$	$2898 \pm 46 \pm 61$
$4.0 < y < 4.5$	$5103 \pm 73 \pm 90$	$1596 \pm 50 \pm 42$

Table 11. Scaled pp differential cross-section in y at $\sqrt{s_{\mathrm{NN}}} = 8.16\,\mathrm{TeV}$. The first uncertainty is statistical, the second is systematic, which includes the systematic uncertainty from the pp measurement and that estimated by changing the interpolation function.

C Nuclear modification factor

Tables 12 and 13 list the nuclear modification factors $R^{\Upsilon(1S)}_{p\mathrm{Pb}}$ for $\Upsilon(1S)$ in transverse momentum bins and in rapidity bins. Tables 14 and 15 listed the nuclear modification factors for $\Upsilon(1S)$ $R^{\Upsilon(2S)}_{p\mathrm{Pb}}$ for $\Upsilon(2S)$ in transverse momentum bins and in rapidity bins. In all tables, the quoted uncertainties are the sum in quadrature of the statistical and systematic components.

p_{T} [GeV/c]	$R_{p\mathrm{Pb}}^{\Upsilon(1S)}$ in pPb	$R_{p\mathrm{Pb}}^{\Upsilon(1S)}$ in Pbp
$0 < p_{\mathrm{T}} < 2$	0.46 ± 0.06	0.76 ± 0.11
$2 < p_{\mathrm{T}} < 4$	0.46 ± 0.05	0.92 ± 0.13
$4 < p_{\mathrm{T}} < 6$	0.66 ± 0.07	0.90 ± 0.13
$6 < p_{\mathrm{T}} < 8$	0.67 ± 0.08	0.91 ± 0.17
$8 < p_{\mathrm{T}} < 10$	0.79 ± 0.10	0.81 ± 0.12
$10 < p_{\mathrm{T}} < 15$	0.84 ± 0.10	1.14 ± 0.16
$15 < p_{\mathrm{T}} < 25$	0.87 ± 0.16	1.04 ± 0.18

Table 12. $\Upsilon(1S)$ nuclear modification factor, $R_{p\mathrm{Pb}}^{\Upsilon(1S)}$, in pPb and Pbp as a function of p_{T} integrated over y^* in the range $1.5 < y^* < 4.0$ for pPb and $-5.0 < y^* < -2.5$ for Pbp.

y^*	$R_{p\mathrm{Pb}}^{\Upsilon(1S)}$
$-4.5 < y^* < -4.0$	1.09 ± 0.14
$-4.0 < y^* < -3.5$	0.82 ± 0.12
$-3.5 < y^* < -3.0$	0.88 ± 0.12
$-3.0 < y^* < -2.5$	1.09 ± 0.13
$2.0 < y^* < 2.5$	0.67 ± 0.06
$2.5 < y^* < 3.0$	0.64 ± 0.06
$3.0 < y^* < 3.5$	0.60 ± 0.07
$3.5 < y^* < 4.0$	0.66 ± 0.10

Table 13. $\Upsilon(1S)$ nuclear modification factor, $R_{p\mathrm{Pb}}^{\Upsilon(1S)}$, in pPb and Pbp as a function of y^* integrated over p_{T} in the range $0 < p_{\mathrm{T}} < 25$ GeV/c.

p_{T} [GeV/c]	$R_{p\mathrm{Pb}}^{\Upsilon(2S)}$ in pPb	$R_{p\mathrm{Pb}}^{\Upsilon(2S)}$ in Pbp
$0 < p_{\mathrm{T}} < 2$	0.22 ± 0.08	0.54 ± 0.17
$2 < p_{\mathrm{T}} < 4$	0.38 ± 0.10	0.55 ± 0.11
$4 < p_{\mathrm{T}} < 6$	0.35 ± 0.09	0.88 ± 0.17
$6 < p_{\mathrm{T}} < 8$	0.30 ± 0.11	0.73 ± 0.31
$8 < p_{\mathrm{T}} < 10$	0.49 ± 0.11	0.48 ± 0.15
$10 < p_{\mathrm{T}} < 15$	0.69 ± 0.12	0.78 ± 0.18
$15 < p_{\mathrm{T}} < 25$	0.78 ± 0.22	0.86 ± 0.35

Table 14. $\Upsilon(2S)$ nuclear modification factor, $R_{p\mathrm{Pb}}^{\Upsilon(2S)}$, in pPb and Pbp as a function of p_{T} integrated over y^* in the range $1.5 < y^* < 4.0$ for pPb and $-5.0 < y^* < -2.5$ for Pbp.

y^*	$R_{p\mathrm{Pb}}^{\Upsilon(2S)}$
$-4.5 < y^* < -4.0$	0.61 ± 0.13
$-4.0 < y^* < -3.5$	0.83 ± 0.16
$-3.5 < y^* < -3.0$	0.72 ± 0.13
$-3.0 < y^* < -2.5$	0.76 ± 0.15
$2.0 < y^* < 2.5$	0.63 ± 0.11
$2.5 < y^* < 3.0$	0.61 ± 0.11
$3.0 < y^* < 3.5$	0.36 ± 0.10
$3.5 < y^* < 4.0$	0.46 ± 0.14

Table 15. $\Upsilon(2S)$ nuclear modification factor, $R_{p\mathrm{Pb}}^{\Upsilon(2S)}$, in pPb and Pbp as a function of y^* integrated over p_{T} in the range $0 < p_{\mathrm{T}} < 25$ GeV/c.

D Forward-to-backward ratios

Tables 16 and 17 list the forward-to-backward ratios $R_{\mathrm{FB}}^{\Upsilon(1S)}$ for $\Upsilon(1S)$ in transverse momentum bins and in rapidity bins. In all tables, the quoted uncertainties are the sum in quadrature of the statistical and systematic components. The ratio $R_{\mathrm{FB}}^{\Upsilon(2S)}$ integrated over $|y^*|$ in the range $2.5 < |y^*| < 4.0$, and over p_{T} in the range $0 < p_{\mathrm{T}} < 25$ GeV/c is 0.66 ± 0.23.

JHEP11(2018)194

p_{T} [GeV/c]	$R_{\mathrm{FB}}^{\Upsilon(1S)}$
$0 < p_{\mathrm{T}} < 2$	0.73 ± 0.19
$2 < p_{\mathrm{T}} < 4$	0.74 ± 0.18
$4 < p_{\mathrm{T}} < 6$	0.92 ± 0.19
$6 < p_{\mathrm{T}} < 8$	1.01 ± 0.19
$8 < p_{\mathrm{T}} < 10$	1.37 ± 0.20
$10 < p_{\mathrm{T}} < 15$	1.22 ± 0.20
$15 < p_{\mathrm{T}} < 25$	1.46 ± 0.26

Table 16. $\Upsilon(1S)$ forward-to-backward ratio, $R_{\mathrm{FB}}^{\Upsilon(1S)}$, as a function of p_{T} integrated over $|y^*|$ in the range $2.5 < |y^*| < 4.0$.

$\lvert y^* \rvert$	$R_{\mathrm{FB}}^{\Upsilon(1S)}$
$2.5 < \lvert y^* \rvert < 3.0$	0.59 ± 0.16
$3.0 < \lvert y^* \rvert < 3.5$	0.68 ± 0.18
$3.5 < \lvert y^* \rvert < 4.0$	0.80 ± 0.21

Table 17. $\Upsilon(1S)$ forward-to-backward ratio, $R_{\mathrm{FB}}^{\Upsilon(1S)}$, as a function of $|y^*|$ integrated over p_{T} in the range $0 < p_{\mathrm{T}} < 25$ GeV/c.

E Ratios between excited states

Tables 18 and 19 list the $\Upsilon(2S)$ to $\Upsilon(1S)$ ratios in bins of transverse momentum bins and rapidity. In all tables, the quoted uncertainties are the sum in quadrature of the statistical and systematic components.

p_{T} [GeV/c]	$R(\Upsilon(2S))$ in pPb	$R(\Upsilon(2S))$ in Pbp
$0 < p_{\mathrm{T}} < 2$	0.20 ± 0.06	0.21 ± 0.07
$2 < p_{\mathrm{T}} < 4$	0.36 ± 0.06	0.25 ± 0.06
$4 < p_{\mathrm{T}} < 6$	0.22 ± 0.05	0.33 ± 0.08
$6 < p_{\mathrm{T}} < 8$	0.26 ± 0.06	0.29 ± 0.09
$8 < p_{\mathrm{T}} < 10$	0.35 ± 0.07	0.28 ± 0.11
$10 < p_{\mathrm{T}} < 15$	0.42 ± 0.08	0.41 ± 0.09
$15 < p_{\mathrm{T}} < 25$	0.55 ± 0.15	0.49 ± 0.19

Table 18. $\Upsilon(2S)$ to $\Upsilon(1S)$ ratio, $R(\Upsilon(2S))$, in pPb and Pbp as a function of p_{T} integrated over y^* in the range $1.5 < y^* < 4.0$ for pPb and $-5.0 < y^* < -2.5$ for Pbp.

JHEP11(2018)194

y^*	$R(2S)$
$-5.0 < y^* < -4.5$	0.27 ± 0.05
$-4.5 < y^* < -4.0$	0.18 ± 0.03
$-4.0 < y^* < -3.5$	0.34 ± 0.06
$-3.5 < y^* < -3.0$	0.28 ± 0.05
$-3.0 < y^* < -2.5$	0.24 ± 0.09
$1.5 < y^* < 2.0$	0.38 ± 0.08
$2.0 < y^* < 2.5$	0.31 ± 0.05
$2.5 < y^* < 3.0$	0.31 ± 0.05
$3.0 < y^* < 3.5$	0.19 ± 0.05
$3.5 < y^* < 4.0$	0.23 ± 0.07

Table 19. $\Upsilon(2S)$ to $\Upsilon(1S)$ ratio, $R(\Upsilon(2S))$, in pPb and Pbp as a function of y^* integrated over p_{T} in the range $0 < p_{\mathrm{T}} < 25$ GeV/c.

F $\Upsilon(1S)$ to nonprompt J/ψ ratios

Table 20 lists the $\Upsilon(1S)$ to nonprompt J/ψ ratios in rapidity bins.

y^*	$\Upsilon(1S)$ to J/ψ-from-b
$-5.0 < y^* < -4.5$	0.125 ± 0.020
$-4.5 < y^* < -4.0$	0.102 ± 0.013
$-4.0 < y^* < -3.5$	0.087 ± 0.013
$-3.5 < y^* < -3.0$	0.094 ± 0.013
$-3.0 < y^* < -2.5$	0.112 ± 0.014
$1.5 < y^* < 2.0$	0.077 ± 0.008
$2.0 < y^* < 2.5$	0.074 ± 0.007
$2.5 < y^* < 3.0$	0.082 ± 0.008
$3.0 < y^* < 3.5$	0.078 ± 0.009
$3.5 < y^* < 4.0$	0.091 ± 0.013

Table 20. $\Upsilon(1S)$ to nonprompt J/ψ, in pPb and Pbp as a function of y^* integrated over p_{T} in the range $0 < p_{\mathrm{T}} < 25$ GeV/c. The quoted uncertainties are the sum in quadrature of the statistical and systematic components.

References

[1] STAR collaboration, J. Adams et al., *Experimental and theoretical challenges in the search for the quark gluon plasma: The STAR Collaboration's critical assessment of the evidence from RHIC collisions*, Nucl. Phys. **A 757** (2005) 102 [nucl-ex/0501009] [INSPIRE].

[2] R. Maciula and A. Szczurek, *Open charm production at the LHC: k_t-factorization approach*, Phys. Rev. **D 87** (2013) 094022 [arXiv:1301.3033] [INSPIRE].

[3] T. Matsui and H. Satz, *J/ψ suppression by quark-gluon plasma formation*, Phys. Lett. **B 178** (1986) 416 [INSPIRE].

[4] D. de Florian, R. Sassot, P. Zurita and M. Stratmann, *Global Analysis of Nuclear Parton Distributions*, Phys. Rev. **D 85** (2012) 074028 [arXiv:1112.6324] [INSPIRE].

[5] J.F. Owens, A. Accardi and W. Melnitchouk, *Global parton distributions with nuclear and finite-Q^2 corrections*, Phys. Rev. **D 87** (2013) 094012 [arXiv:1212.1702] [INSPIRE].

[6] K.J. Eskola, H. Paukkunen and C.A. Salgado, *EPS09: A New Generation of NLO and LO Nuclear Parton Distribution Functions*, JHEP **04** (2009) 065 [arXiv:0902.4154] [INSPIRE].

[7] K. Kovarik et al., *nCTEQ15 — Global analysis of nuclear parton distributions with uncertainties in the CTEQ framework*, Phys. Rev. **D 93** (2016) 085037 [arXiv:1509.00792] [INSPIRE].

[8] F. Arleo and S. Peigné, *Quarkonium suppression in heavy-ion collisions from coherent energy loss in cold nuclear matter*, JHEP **10** (2014) 073 [arXiv:1407.5054] [INSPIRE].

[9] F. Arleo, R. Kolevatov, S. Peigné and M. Rustamova, *Centrality and* $p_\perp$ *dependence of* J/ψ *suppression in proton-nucleus collisions from parton energy loss*, JHEP **05** (2013) 155 [`arXiv:1304.0901`] [INSPIRE].

[10] F. Arleo and S. Peigné, *Heavy-quarkonium suppression in p-A collisions from parton energy loss in cold QCD matter*, JHEP **03** (2013) 122 [`arXiv:1212.0434`] [INSPIRE].

[11] C. Gerschel and J. Hüfner, *A contribution to the suppression of the* J/ψ *meson produced in high-energy nucleus-nucleus collisions*, Phys. Lett. **B 207** (1988) 253 [INSPIRE].

[12] J.L. Albacete et al., *Predictions for p+Pb collisions at* $\sqrt{s_{NN}} = 5\,TeV$, Int. J. Mod. Phys. **E 22** (2013) 1330007 [`arXiv:1301.3395`] [INSPIRE].

[13] A. Adeluyi and T. Nguyen, *Coherent photoproduction of* ψ *and* Υ *mesons in ultraperipheral pPb and PbPb collisions at the CERN Large Hadron Collider at* $\sqrt{s_{NN}} = 5$ *TeV and* $\sqrt{s_{NN}} = 2.76$ *TeV*, Phys. Rev. **C 87** (2013) 027901 [`arXiv:1302.4288`] [INSPIRE].

[14] G.A. Chirilli, B.-W. Xiao and F. Yuan, *Inclusive hadron productions in pA collisions*, Phys. Rev. **D 86** (2012) 054005 [`arXiv:1203.6139`] [INSPIRE].

[15] G.A. Chirilli, *High-Energy QCD factorization from DIS to pA collisions*, Int. J. Mod. Phys. Conf. Ser. **20** (2012) 200 [`arXiv:1209.1614`] [INSPIRE].

[16] E.G. Ferreiro, F. Fleuret, J.P. Lansberg and A. Rakotozafindrabe, *Impact of the nuclear modification of the gluon densities on* J/ψ *production in pPb collisions at* $\sqrt{s_{NN}} = 5\,TeV$, Phys. Rev. **C 88** (2013) 047901 [`arXiv:1305.4569`] [INSPIRE].

[17] E.G. Ferreiro and J.-P. Lansberg, *Is bottomonium suppression in proton-nucleus and nucleus-nucleus collisions at LHC energies due to the same effects?*, JHEP **10** (2018) 094 [`arXiv:1804.04474`] [INSPIRE].

[18] E.G. Ferreiro, *Excited charmonium suppression in proton-nucleus collisions as a consequence of comovers*, Phys. Lett. **B 749** (2015) 98 [`arXiv:1411.0549`] [INSPIRE].

[19] X. Du and R. Rapp, *Sequential Regeneration of Charmonia in Heavy-Ion Collisions*, Nucl. Phys. **A 943** (2015) 147 [`arXiv:1504.00670`] [INSPIRE].

[20] Y.-Q. Ma, R. Venugopalan, K. Watanabe and H.-F. Zhang, $\psi(2S)$ *versus* J/ψ *suppression in proton-nucleus collisions from factorization violating soft color exchanges*, Phys. Rev. **C 97** (2018) 014909 [`arXiv:1707.07266`] [INSPIRE].

[21] CMS collaboration, *Indications of suppression of excited* Υ *states in PbPb collisions at* $\sqrt{S_{NN}} = 2.76\,TeV$, Phys. Rev. Lett. **107** (2011) 052302 [`arXiv:1105.4894`] [INSPIRE].

[22] ATLAS collaboration, *Measurement of quarkonium production in proton-lead and proton-proton collisions at* 5.02 *TeV with the ATLAS detector*, Eur. Phys. J. **C 78** (2018) 171 [`arXiv:1709.03089`] [INSPIRE].

[23] STAR collaboration, Z. Ye, Υ *measurements in p+p, p+Au and Au+Au collisions at* $\sqrt{s_{NN}} = 200\,GeV$ *with the STAR experiment*, Nucl. Phys. **A 967** (2017) 600 [INSPIRE].

[24] CMS collaboration, *Suppression of* $\Upsilon(1S), \Upsilon(2S)$ *and* $\Upsilon(3S)$ *quarkonium states in PbPb collisions at* $\sqrt{s_{NN}} = 2.76\,TeV$, Phys. Lett. **B 770** (2017) 357 [`arXiv:1611.01510`] [INSPIRE].

[25] CMS collaboration, *Event activity dependence of* $\Upsilon(nS)$ *production in* $\sqrt{s_{\rm NN}} = 5.02\,TeV$ *pPb and* $\sqrt{s} = 2.76\,TeV$ *pp collisions*, JHEP **04** (2014) 103 [`arXiv:1312.6300`] [INSPIRE].

[26] CMS collaboration, *Suppression of excited* Υ *states relative to the ground state in Pb-Pb collisions at* $\sqrt{s_{NN}} = 5.02\,TeV$, Phys. Rev. Lett. **120** (2018) 142301 [`arXiv:1706.05984`] [INSPIRE].

[27] ALICE collaboration, *Production of inclusive $\Upsilon(1S)$ and $\Upsilon(2S)$ in p-Pb collisions at $\sqrt{s_{\rm NN}} = 5.02$ TeV*, Phys. Lett. **B 740** (2015) 105 [arXiv:1410.2234] [INSPIRE].

[28] LHCb collaboration, *Study of Υ production and cold nuclear matter effects in pPb collisions at $\sqrt{s_{NN}} = 5$ TeV*, JHEP **07** (2014) 094 [arXiv:1405.5152] [INSPIRE].

[29] LHCb collaboration, *Prompt and nonprompt J/ψ production and nuclear modification in pPb collisions at $\sqrt{s_{\rm NN}} = 8.16$ TeV*, Phys. Lett. **B 774** (2017) 159 [arXiv:1706.07122] [INSPIRE].

[30] LHCb collaboration, *The LHCb detector at the LHC*, 2008 JINST **3** S08005 [INSPIRE].

[31] LHCb collaboration, *LHCb detector performance*, Int. J. Mod. Phys. **A 30** (2015) 1530022 [arXiv:1412.6352] [INSPIRE].

[32] R. Aaij et al., *Performance of the LHCb Vertex Locator*, 2014 JINST **9** P09007 [arXiv:1405.7808] [INSPIRE].

[33] R. Arink et al., *Performance of the LHCb Outer Tracker*, 2014 JINST **9** P01002 [arXiv:1311.3893] [INSPIRE].

[34] M. Adinolfi et al., *Performance of the LHCb RICH detector at the LHC*, Eur. Phys. J. **C 73** (2013) 2431 [arXiv:1211.6759] [INSPIRE].

[35] A.A. Alves Jr. et al., *Performance of the LHCb muon system*, 2013 JINST **8** P02022 [arXiv:1211.1346] [INSPIRE].

[36] R. Aaij et al., *The LHCb trigger and its performance in 2011*, 2013 JINST **8** P04022 [arXiv:1211.3055] [INSPIRE].

[37] G. Dujany and B. Storaci, *Real-time alignment and calibration of the LHCb Detector in Run II*, J. Phys. Conf. Ser. **664** (2015) 082010 [INSPIRE].

[38] R. Aaij et al., *Tesla: an application for real-time data analysis in High Energy Physics*, Comput. Phys. Commun. **208** (2016) 35 [arXiv:1604.05596] [INSPIRE].

[39] LHCb collaboration, *Study of J/ψ production in jets*, Phys. Rev. Lett. **118** (2017) 192001 [arXiv:1701.05116] [INSPIRE].

[40] T. Pierog, I. Karpenko, J.M. Katzy, E. Yatsenko and K. Werner, *EPOS LHC: Test of collective hadronization with data measured at the CERN Large Hadron Collider*, Phys. Rev. **C 92** (2015) 034906 [arXiv:1306.0121] [INSPIRE].

[41] T. Sjöstrand, S. Mrenna and P.Z. Skands, *PYTHIA 6.4 physics and manual*, JHEP **05** (2006) 026 [hep-ph/0603175] [INSPIRE].

[42] T. Sjöstrand, S. Mrenna and P.Z. Skands, *A brief introduction to PYTHIA 8.1*, Comput. Phys. Commun. **178** (2008) 852 [arXiv:0710.3820] [INSPIRE].

[43] GEANT4 collaboration, J. Allison et al., *Geant4 developments and applications*, IEEE Trans. Nucl. Sci. **53** (2006) 270.

[44] GEANT4 collaboration, S. Agostinelli et al., *Geant4: A simulation toolkit*, Nucl. Instrum. Meth. **A 506** (2003) 250 [INSPIRE].

[45] M. Clemencic et al., *The LHCb simulation application, Gauss: Design, evolution and experience*, J. Phys. Conf. Ser. **331** (2011) 032023 [INSPIRE].

[46] LHCb collaboration, *Measurement of the Υ polarizations in pp collisions at $\sqrt{s_{NN}} = 7$ and 8 TeV*, JHEP **12** (2017) 110 [arXiv:1709.01301] [INSPIRE].

[47] LHCb collaboration, *Precision luminosity measurements at LHCb*, 2014 JINST **9** P12005 [arXiv:1410.0149] [INSPIRE].

[48] Particle Data Group collaboration, M. Tanabashi et al., *Review of Particle Physics*, *Phys. Rev.* **D 98** (2018) 030001 [inSPIRE].

[49] T. Skwarnicki, *A study of the radiative cascade transitions between the Upsilon-prime and Upsilon resonances*, Ph.D. Thesis, Institute of Nuclear Physics, Krakow (1986) [DESY-F31-86-02] [inSPIRE].

[50] LHCb collaboration, *Measurement of Υ production in pp collisions at $\sqrt{s} = 2.76$ TeV*, *Eur. Phys. J.* **C 74** (2014) 2835 [`arXiv:1402.2539`] [inSPIRE].

[51] LHCb collaboration, *Forward production of Υ mesons in pp collisions at $\sqrt{s} = 7$ and 8 TeV*, *JHEP* **11** (2015) 103 [`arXiv:1509.02372`] [inSPIRE].

[52] LHCb collaboration, *Measurement of Υ production cross-section in pp collisions at $\sqrt{s} = 13$ TeV*, *JHEP* **07** (2018) 134 [`arXiv:1804.09214`] [inSPIRE].

[53] J.-P. Lansberg and H.-S. Shao, *Towards an automated tool to evaluate the impact of the nuclear modification of the gluon density on quarkonium, D and B meson production in proton-nucleus collisions*, *Eur. Phys. J.* **C 77** (2017) 1 [`arXiv:1610.05382`] [inSPIRE].

[54] H.-S. Shao, *HELAC-Onia 2.0: An upgraded matrix-element and event generator for heavy quarkonium physics*, *Comput. Phys. Commun.* **198** (2016) 238 [`arXiv:1507.03435`] [inSPIRE].

[55] H.-S. Shao, *HELAC-Onia: An automatic matrix element generator for heavy quarkonium physics*, *Comput. Phys. Commun.* **184** (2013) 2562 [`arXiv:1212.5293`] [inSPIRE].

[56] K.J. Eskola, P. Paakkinen, H. Paukkunen and C.A. Salgado, *EPPS16 — Bringing nuclear PDFs to the LHC era*, in *12th International Workshop on High-pT Physics in the RHIC/LHC Era (HPT 2017)*, Bergen, Norway, October 2–5, 2017 (2018) [`arXiv:1802.00713`] [inSPIRE].

[57] X. Yao and B. Müller, *Approach to equilibrium of quarkonium in quark-gluon plasma*, *Phys. Rev.* **C 97** (2018) 014908 [*Erratum ibid.* **C 97** (2018) 049903] [`arXiv:1709.03529`] [inSPIRE].

[58] M. Winn, *Prospects for quarkonium measurements in p-A and A-A collisions at the LHC*, *Few Body Syst.* **58** (2017) 53 [`arXiv:1609.01135`] [inSPIRE].

The LHCb collaboration

R. Aaij[28], C. Abellán Beteta[45], B. Adeva[42], M. Adinolfi[49], C.A. Aidala[76], Z. Ajaltouni[6], S. Akar[60], P. Albicocco[19], J. Albrecht[11], F. Alessio[43], M. Alexander[54], A. Alfonso Albero[41], G. Alkhazov[34], P. Alvarez Cartelle[56], A.A. Alves Jr[42], S. Amato[2], S. Amerio[24], Y. Amhis[8], L. An[3], L. Anderlini[18], G. Andreassi[44], M. Andreotti[17], J.E. Andrews[61], R.B. Appleby[57], F. Archilli[28], P. d'Argent[13], J. Arnau Romeu[7], A. Artamonov[40], M. Artuso[62], K. Arzymatov[38], E. Aslanides[7], M. Atzeni[45], B. Audurier[23], S. Bachmann[13], J.J. Back[51], S. Baker[56], V. Balagura[8,b], W. Baldini[17], A. Baranov[38], R.J. Barlow[57], S. Barsuk[8], W. Barter[57], M. Bartolini[20], F. Baryshnikov[73], V. Batozskaya[32], B. Batsukh[62], A. Battig[11], V. Battista[44], A. Bay[44], J. Beddow[54], F. Bedeschi[25], I. Bediaga[1], A. Beiter[62], L.J. Bel[28], S. Belin[23], N. Beliy[65], V. Bellee[44], N. Belloli[21,i], K. Belous[40], I. Belyaev[35], E. Ben-Haim[9], G. Bencivenni[19], S. Benson[28], S. Beranek[10], A. Berezhnoy[36], R. Bernet[45], D. Berninghoff[13], E. Bertholet[9], A. Bertolin[24], C. Betancourt[45], F. Betti[16,43], M.O. Bettler[50], M. van Beuzekom[28], Ia. Bezshyiko[45], S. Bhasin[49], J. Bhom[30], S. Bifani[48], P. Billoir[9], A. Birnkraut[11], A. Bizzeti[18,u], M. Bjørn[58], M.P. Blago[43], T. Blake[51], F. Blanc[44], S. Blusk[62], D. Bobulska[54], V. Bocci[27], O. Boente Garcia[42], T. Boettcher[59], A. Bondar[39,w], N. Bondar[34], S. Borghi[57,43], M. Borisyak[38], M. Borsato[42], F. Bossu[8], M. Boubdir[10], T.J.V. Bowcock[55], C. Bozzi[17,43], S. Braun[13], M. Brodski[43], J. Brodzicka[30], A. Brossa Gonzalo[51], D. Brundu[23,43], E. Buchanan[49], A. Buonaura[45], C. Burr[57], A. Bursche[23], J. Buytaert[43], W. Byczynski[43], S. Cadeddu[23], H. Cai[67], R. Calabrese[17,g], R. Calladine[48], M. Calvi[21,i], M. Calvo Gomez[41,m], A. Camboni[41,m], P. Campana[19], D.H. Campora Perez[43], L. Capriotti[16], A. Carbone[16,e], G. Carboni[26], R. Cardinale[20], A. Cardini[23], P. Carniti[21,i], L. Carson[53], K. Carvalho Akiba[2], G. Casse[55], L. Cassina[21], M. Cattaneo[43], G. Cavallero[20,h], R. Cenci[25,p], D. Chamont[8], M.G. Chapman[49], M. Charles[9], Ph. Charpentier[43], G. Chatzikonstantinidis[48], M. Chefdeville[5], V. Chekalina[38], C. Chen[3], S. Chen[23], S.-G. Chitic[43], V. Chobanova[42], M. Chrzaszcz[43], A. Chubykin[34], P. Ciambrone[19], X. Cid Vidal[42], G. Ciezarek[43], P.E.L. Clarke[53], M. Clemencic[43], H.V. Cliff[50], J. Closier[43], V. Coco[43], J.A.B. Coelho[8], J. Cogan[7], E. Cogneras[6], L. Cojocariu[33], P. Collins[43], T. Colombo[43], A. Comerma-Montells[13], A. Contu[23], G. Coombs[43], S. Coquereau[41], G. Corti[43], M. Corvo[17,g], C.M. Costa Sobral[51], B. Couturier[43], G.A. Cowan[53], D.C. Craik[59], A. Crocombe[51], M. Cruz Torres[1], R. Currie[53], C. D'Ambrosio[43], F. Da Cunha Marinho[2], C.L. Da Silva[77], E. Dall'Occo[28], J. Dalseno[49], A. Danilina[35], A. Davis[3], O. De Aguiar Francisco[43], K. De Bruyn[43], S. De Capua[57], M. De Cian[44], J.M. De Miranda[1], L. De Paula[2], M. De Serio[15,d], P. De Simone[19], C.T. Dean[54], D. Decamp[5], L. Del Buono[9], B. Delaney[50], H.-P. Dembinski[12], M. Demmer[11], A. Dendek[31], D. Derkach[38], O. Deschamps[6], F. Desse[8], F. Dettori[55], B. Dey[68], A. Di Canto[43], P. Di Nezza[19], S. Didenko[73], H. Dijkstra[43], F. Dordei[43], M. Dorigo[43,y], A. Dosil Suárez[42], L. Douglas[54], A. Dovbnya[46], K. Dreimanis[55], L. Dufour[28], G. Dujany[9], P. Durante[43], J.M. Durham[77], D. Dutta[57], R. Dzhelyadin[40], M. Dziewiecki[13], A. Dziurda[30], A. Dzyuba[34], S. Easo[52], U. Egede[56], V. Egorychev[35], S. Eidelman[39,w], S. Eisenhardt[53], U. Eitschberger[11], R. Ekelhof[11], L. Eklund[54], S. Ely[62], A. Ene[33], S. Escher[10], S. Esen[28], T. Evans[60], A. Falabella[16], N. Farley[48], S. Farry[55], D. Fazzini[21,43,i], L. Federici[26], P. Fernandez Declara[43], A. Fernandez Prieto[42], F. Ferrari[16], L. Ferreira Lopes[44], F. Ferreira Rodrigues[2], M. Ferro-Luzzi[43], S. Filippov[37], R.A. Fini[15], M. Fiorini[17,g], M. Firlej[31], C. Fitzpatrick[44], T. Fiutowski[31], F. Fleuret[8,b], M. Fontana[43], F. Fontanelli[20,h], R. Forty[43], V. Franco Lima[55], M. Frank[43], C. Frei[43], J. Fu[22,q], W. Funk[43], C. Färber[43], M. Féo Pereira Rivello Carvalho[28], E. Gabriel[53], A. Gallas Torreira[42], D. Galli[16,e], S. Gallorini[24], S. Gambetta[53], Y. Gan[3], M. Gandelman[2], P. Gandini[22], Y. Gao[3], L.M. Garcia Martin[75], B. Garcia Plana[42], J. García Pardiñas[45], J. Garra Tico[50], L. Garrido[41], D. Gascon[41], C. Gaspar[43], L. Gavardi[11], G. Gazzoni[6], D. Gerick[13],

E. Gersabeck^{57}, M. Gersabeck^{57}, T. Gershon^{51}, D. Gerstel^{7}, Ph. Ghez^{5}, V. Gibson^{50}, O.G. Girard^{44}, P. Gironella Gironell^{41}, L. Giubega^{33}, K. Gizdov^{53}, V.V. Gligorov^{9}, D. Golubkov^{35}, A. Golutvin^{56,73}, A. Gomes^{1,a}, I.V. Gorelov^{36}, C. Gotti^{21,i}, E. Govorkova^{28}, J.P. Grabowski^{13}, R. Graciani Diaz^{41}, L.A. Granado Cardoso^{43}, E. Graugés^{41}, E. Graverini^{45}, G. Graziani^{18}, A. Grecu^{33}, R. Greim^{28}, P. Griffith^{23}, L. Grillo^{57}, L. Gruber^{43}, B.R. Gruberg Cazon^{58}, O. Grünberg^{70}, C. Gu^{3}, E. Gushchin^{37}, A. Guth^{10}, Yu. Guz^{40,43}, T. Gys^{43}, C. Göbel^{64}, T. Hadavizadeh^{58}, C. Hadjivasiliou^{6}, G. Haefeli^{44}, C. Haen^{43}, S.C. Haines^{50}, B. Hamilton^{61}, X. Han^{13}, T.H. Hancock^{58}, S. Hansmann-Menzemer^{13}, N. Harnew^{58}, S.T. Harnew^{49}, T. Harrison^{55}, C. Hasse^{43}, M. Hatch^{43}, J. He^{65}, M. Hecker^{56}, K. Heinicke^{11}, A. Heister^{11}, K. Hennessy^{55}, L. Henry^{75}, E. van Herwijnen^{43}, J. Heuel^{10}, M. Heß^{70}, A. Hicheur^{63}, R. Hidalgo Charman^{57}, D. Hill^{58}, M. Hilton^{57}, P.H. Hopchev^{44}, J. Hu^{13}, W. Hu^{68}, W. Huang^{65}, Z.C. Huard^{60}, W. Hulsbergen^{28}, T. Humair^{56}, M. Hushchyn^{38}, D. Hutchcroft^{55}, D. Hynds^{28}, P. Ibis^{11}, M. Idzik^{31}, P. Ilten^{48}, K. Ivshin^{34}, R. Jacobsson^{43}, J. Jalocha^{58}, E. Jans^{28}, A. Jawahery^{61}, F. Jiang^{3}, M. John^{58}, D. Johnson^{43}, C.R. Jones^{50}, C. Joram^{43}, B. Jost^{43}, N. Jurik^{58}, S. Kandybei^{46}, M. Karacson^{43}, J.M. Kariuki^{49}, S. Karodia^{54}, N. Kazeev^{38}, M. Kecke^{13}, F. Keizer^{50}, M. Kelsey^{62}, M. Kenzie^{50}, T. Ketel^{29}, E. Khairullin^{38}, B. Khanji^{43}, C. Khurewathanakul^{44}, K.E. Kim^{62}, T. Kirn^{10}, S. Klaver^{19}, K. Klimaszewski^{32}, T. Klimkovich^{12}, S. Koliiev^{47}, M. Kolpin^{13}, R. Kopecna^{13}, P. Koppenburg^{28}, I. Kostiuk^{28}, S. Kotriakhova^{34}, M. Kozeiha^{6}, L. Kravchuk^{37}, M. Kreps^{51}, F. Kress^{56}, P. Krokovny^{39,w}, W. Krupa^{31}, W. Krzemien^{32}, W. Kucewicz^{30,l}, M. Kucharczyk^{30}, V. Kudryavtsev^{39,w}, A.K. Kuonen^{44}, T. Kvaratskheliya^{35,43}, D. Lacarrere^{43}, G. Lafferty^{57}, A. Lai^{23}, D. Lancierini^{45}, G. Lanfranchi^{19}, C. Langenbruch^{10}, T. Latham^{51}, C. Lazzeroni^{48}, R. Le Gac^{7}, A. Leflat^{36}, J. Lefrançois^{8}, R. Lefèvre^{6}, F. Lemaitre^{43}, O. Leroy^{7}, T. Lesiak^{30}, B. Leverington^{13}, P.-R. Li^{65}, Y. Li^{4}, Z. Li^{62}, X. Liang^{62}, T. Likhomanenko^{72}, R. Lindner^{43}, F. Lionetto^{45}, V. Lisovskyi^{8}, G. Liu^{66}, X. Liu^{3}, D. Loh^{51}, A. Loi^{23}, I. Longstaff^{54}, J.H. Lopes^{2}, G.H. Lovell^{50}, D. Lucchesi^{24,o}, M. Lucio Martinez^{42}, A. Lupato^{24}, E. Luppi^{17,g}, O. Lupton^{43}, A. Lusiani^{25}, X. Lyu^{65}, F. Machefert^{8}, F. Maciuc^{33}, V. Macko^{44}, P. Mackowiak^{11}, S. Maddrell-Mander^{49}, O. Maev^{34,43}, K. Maguire^{57}, D. Maisuzenko^{34}, M.W. Majewski^{31}, S. Malde^{58}, B. Malecki^{30}, A. Malinin^{72}, T. Maltsev^{39,w}, G. Manca^{23,f}, G. Mancinelli^{7}, D. Marangotto^{22,q}, J. Maratas^{6,v}, J.F. Marchand^{5}, U. Marconi^{16}, C. Marin Benito^{8}, M. Marinangeli^{44}, P. Marino^{44}, J. Marks^{13}, P.J. Marshall^{55}, G. Martellotti^{27}, M. Martin^{7}, M. Martinelli^{43}, D. Martinez Santos^{42}, F. Martinez Vidal^{75}, A. Massafferri^{1}, M. Materok^{10}, R. Matev^{43}, A. Mathad^{51}, Z. Mathe^{43}, C. Matteuzzi^{21}, A. Mauri^{45}, E. Maurice^{8,b}, B. Maurin^{44}, A. Mazurov^{48}, M. McCann^{56,43}, A. McNab^{57}, R. McNulty^{14}, J.V. Mead^{55}, B. Meadows^{60}, C. Meaux^{7}, N. Meinert^{70}, D. Melnychuk^{32}, M. Merk^{28}, A. Merli^{22,q}, E. Michielin^{24}, D.A. Milanes^{69}, E. Millard^{51}, M.-N. Minard^{5}, L. Minzoni^{17,g}, D.S. Mitzel^{13}, A. Mogini^{9}, R.D. Moise^{56}, T. Mombächer^{11}, I.A. Monroy^{69}, S. Monteil^{6}, M. Morandin^{24}, G. Morello^{19}, M.J. Morello^{25,t}, O. Morgunova^{72}, J. Moron^{31}, A.B. Morris^{7}, R. Mountain^{62}, F. Muheim^{53}, M. Mulder^{28}, C.H. Murphy^{58}, D. Murray^{57}, A. Mödden ^{11}, D. Müller^{43}, J. Müller^{11}, K. Müller^{45}, V. Müller^{11}, P. Naik^{49}, T. Nakada^{44}, R. Nandakumar^{52}, A. Nandi^{58}, T. Nanut^{44}, I. Nasteva^{2}, M. Needham^{53}, N. Neri^{22}, S. Neubert^{13}, N. Neufeld^{43}, M. Neuner^{13}, R. Newcombe^{56}, T.D. Nguyen^{44}, C. Nguyen-Mau^{44,n}, S. Nieswand^{10}, R. Niet^{11}, N. Nikitin^{36}, A. Nogay^{72}, N.S. Nolte^{43}, D.P. O'Hanlon^{16}, A. Oblakowska-Mucha^{31}, V. Obraztsov^{40}, S. Ogilvy^{19}, R. Oldeman^{23,f}, C.J.G. Onderwater^{71}, A. Ossowska^{30}, J.M. Otalora Goicochea^{2}, P. Owen^{45}, A. Oyanguren^{75}, P.R. Pais^{44}, T. Pajero^{25,t}, A. Palano^{15}, M. Palutan^{19}, G. Panshin^{74}, A. Papanestis^{52}, M. Pappagallo^{53}, L.L. Pappalardo^{17,g}, W. Parker^{61}, C. Parkes^{57,43}, G. Passaleva^{18,43}, A. Pastore^{15}, M. Patel^{56}, C. Patrignani^{16,e}, A. Pearce^{43}, A. Pellegrino^{28}, G. Penso^{27}, M. Pepe Altarelli^{43}, S. Perazzini^{43}, D. Pereima^{35}, P. Perret^{6}, L. Pescatore^{44}, K. Petridis^{49}, A. Petrolini^{20,h}, A. Petrov^{72}, S. Petrucci^{53}, M. Petruzzo^{22,q},

JHEP11(2018)194

B. Pietrzyk[5], G. Pietrzyk[44], M. Pikies[30], M. Pili[58], D. Pinci[27], J. Pinzino[43], F. Pisani[43], A. Piucci[13], V. Placinta[33], S. Playfer[53], J. Plews[48], M. Plo Casasus[42], F. Polci[9], M. Poli Lener[19], A. Poluektov[51], N. Polukhina[73,c], I. Polyakov[62], E. Polycarpo[2], G.J. Pomery[49], S. Ponce[43], A. Popov[40], D. Popov[48,12], S. Poslavskii[40], C. Potterat[2], E. Price[49], J. Prisciandaro[42], C. Prouve[49], V. Pugatch[47], A. Puig Navarro[45], H. Pullen[58], G. Punzi[25,p], W. Qian[65], J. Qin[65], R. Quagliani[9], B. Quintana[6], B. Rachwal[31], J.H. Rademacker[49], M. Rama[25], M. Ramos Pernas[42], M.S. Rangel[2], F. Ratnikov[38,x], G. Raven[29], M. Ravonel Salzgeber[43], M. Reboud[5], F. Redi[44], S. Reichert[11], A.C. dos Reis[1], F. Reiss[9], C. Remon Alepuz[75], Z. Ren[3], V. Renaudin[8], S. Ricciardi[52], S. Richards[49], K. Rinnert[55], P. Robbe[8], A. Robert[9], A.B. Rodrigues[44], E. Rodrigues[60], J.A. Rodriguez Lopez[69], M. Roehrken[43], S. Roiser[43], A. Rollings[58], V. Romanovskiy[40], A. Romero Vidal[42], M. Rotondo[19], M.S. Rudolph[62], T. Ruf[43], J. Ruiz Vidal[75], J.J. Saborido Silva[42], N. Sagidova[34], B. Saitta[23,f], V. Salustino Guimaraes[64], C. Sanchez Gras[28], C. Sanchez Mayordomo[75], B. Sanmartin Sedes[42], R. Santacesaria[27], C. Santamarina Rios[42], M. Santimaria[19,43], E. Santovetti[26,j], G. Sarpis[57], A. Sarti[19,k], C. Satriano[27,s], A. Satta[26], M. Saur[65], D. Savrina[35,36], S. Schael[10], M. Schellenberg[11], M. Schiller[54], H. Schindler[43], M. Schmelling[12], T. Schmelzer[11], B. Schmidt[43], O. Schneider[44], A. Schopper[43], H.F. Schreiner[60], M. Schubiger[44], M.H. Schune[8], R. Schwemmer[43], B. Sciascia[19], A. Sciubba[27,k], A. Semennikov[35], E.S. Sepulveda[9], A. Sergi[48,43], N. Serra[45], J. Serrano[7], L. Sestini[24], A. Seuthe[11], P. Seyfert[43], M. Shapkin[40], Y. Shcheglov[34,†], T. Shears[55], L. Shekhtman[39,w], V. Shevchenko[72], E. Shmanin[73], B.G. Siddi[17], R. Silva Coutinho[45], L. Silva de Oliveira[2], G. Simi[24,o], S. Simone[15,d], I. Skiba[17], N. Skidmore[13], T. Skwarnicki[62], M.W. Slater[48], J.G. Smeaton[50], E. Smith[10], I.T. Smith[53], M. Smith[56], M. Soares[16], l. Soares Lavra[1], M.D. Sokoloff[60], F.J.P. Soler[54], B. Souza De Paula[2], B. Spaan[11], E. Spadaro Norella[22,q], P. Spradlin[54], F. Stagni[43], M. Stahl[13], S. Stahl[43], P. Stefko[44], S. Stefkova[56], O. Steinkamp[45], S. Stemmle[13], O. Stenyakin[40], M. Stepanova[34], H. Stevens[11], A. Stocchi[8], S. Stone[62], B. Storaci[45], S. Stracka[25], M.E. Stramaglia[44], M. Straticiuc[33], U. Straumann[45], S. Strokov[74], J. Sun[3], L. Sun[67], K. Swientek[31], A. Szabelski[32], T. Szumlak[31], M. Szymanski[65], S. T'Jampens[5], Z. Tang[3], A. Tayduganov[7], T. Tekampe[11], G. Tellarini[17], F. Teubert[43], E. Thomas[43], J. van Tilburg[28], M.J. Tilley[56], V. Tisserand[6], M. Tobin[31], S. Tolk[43], L. Tomassetti[17,g], D. Tonelli[25], D.Y. Tou[9], R. Tourinho Jadallah Aoude[1], E. Tournefier[5], M. Traill[54], M.T. Tran[44], A. Trisovic[50], A. Tsaregorodtsev[7], G. Tuci[25,p], A. Tully[50], N. Tuning[28,43], A. Ukleja[32], A. Usachov[8], A. Ustyuzhanin[38], U. Uwer[13], A. Vagner[74], V. Vagnoni[16], A. Valassi[43], S. Valat[43], G. Valenti[16], R. Vazquez Gomez[43], P. Vazquez Regueiro[42], S. Vecchi[17], M. van Veghel[28], J.J. Velthuis[49], M. Veltri[18,r], G. Veneziano[58], A. Venkateswaran[62], M. Vernet[6], M. Veronesi[28], N.V. Veronika[14], M. Vesterinen[58], J.V. Viana Barbosa[43], D. Vieira[65], M. Vieites Diaz[42], H. Viemann[70], X. Vilasis-Cardona[41,m], A. Vitkovskiy[28], M. Vitti[50], V. Volkov[36], A. Vollhardt[45], D. Vom Bruch[9], B. Voneki[43], A. Vorobyev[34], V. Vorobyev[39,w], J.A. de Vries[28], C. Vázquez Sierra[28], R. Waldi[70], J. Walsh[25], J. Wang[4], M. Wang[3], Y. Wang[68], Z. Wang[45], D.R. Ward[50], H.M. Wark[55], N.K. Watson[48], D. Websdale[56], A. Weiden[45], C. Weisser[59], M. Whitehead[10], J. Wicht[51], G. Wilkinson[58], M. Wilkinson[62], I. Williams[50], M.R.J. Williams[57], M. Williams[59], T. Williams[48], F.F. Wilson[52], M. Winn[8], W. Wislicki[32], M. Witek[30], G. Wormser[8], S.A. Wotton[50], K. Wyllie[43], D. Xiao[68], Y. Xie[68], A. Xu[3], M. Xu[68], Q. Xu[65], Z. Xu[3], Z. Xu[5], Z. Yang[3], Z. Yang[61], Y. Yao[62], L.E. Yeomans[55], H. Yin[68], J. Yu[68,aa], X. Yuan[62], O. Yushchenko[40], K.A. Zarebski[48], M. Zavertyaev[12,c], D. Zhang[68], L. Zhang[3], W.C. Zhang[3,z], Y. Zhang[8], A. Zhelezov[13], Y. Zheng[65], X. Zhu[3], V. Zhukov[10,36], J.B. Zonneveld[53], S. Zucchelli[16]

[1] *Centro Brasileiro de Pesquisas Físicas (CBPF), Rio de Janeiro, Brazil*
[2] *Universidade Federal do Rio de Janeiro (UFRJ), Rio de Janeiro, Brazil*

[3] Center for High Energy Physics, Tsinghua University, Beijing, China
[4] Institute Of High Energy Physics (ihep), Beijing, China
[5] Univ. Grenoble Alpes, Univ. Savoie Mont Blanc, CNRS, IN2P3-LAPP, Annecy, France
[6] Clermont Université, Université Blaise Pascal, CNRS/IN2P3, LPC, Clermont-Ferrand, France
[7] Aix Marseille Univ, CNRS/IN2P3, CPPM, Marseille, France
[8] LAL, Univ. Paris-Sud, CNRS/IN2P3, Université Paris-Saclay, Orsay, France
[9] LPNHE, Sorbonne Université, Paris Diderot Sorbonne Paris Cité, CNRS/IN2P3, Paris, France
[10] I. Physikalisches Institut, RWTH Aachen University, Aachen, Germany
[11] Fakultät Physik, Technische Universität Dortmund, Dortmund, Germany
[12] Max-Planck-Institut für Kernphysik (MPIK), Heidelberg, Germany
[13] Physikalisches Institut, Ruprecht-Karls-Universität Heidelberg, Heidelberg, Germany
[14] School of Physics, University College Dublin, Dublin, Ireland
[15] INFN Sezione di Bari, Bari, Italy
[16] INFN Sezione di Bologna, Bologna, Italy
[17] INFN Sezione di Ferrara, Ferrara, Italy
[18] INFN Sezione di Firenze, Firenze, Italy
[19] INFN Laboratori Nazionali di Frascati, Frascati, Italy
[20] INFN Sezione di Genova, Genova, Italy
[21] INFN Sezione di Milano-Bicocca, Milano, Italy
[22] INFN Sezione di Milano, Milano, Italy
[23] INFN Sezione di Cagliari, Monserrato, Italy
[24] INFN Sezione di Padova, Padova, Italy
[25] INFN Sezione di Pisa, Pisa, Italy
[26] INFN Sezione di Roma Tor Vergata, Roma, Italy
[27] INFN Sezione di Roma La Sapienza, Roma, Italy
[28] Nikhef National Institute for Subatomic Physics, Amsterdam, Netherlands
[29] Nikhef National Institute for Subatomic Physics and VU University Amsterdam, Amsterdam, Netherlands
[30] Henryk Niewodniczanski Institute of Nuclear Physics Polish Academy of Sciences, Kraków, Poland
[31] AGH - University of Science and Technology, Faculty of Physics and Applied Computer Science, Kraków, Poland
[32] National Center for Nuclear Research (NCBJ), Warsaw, Poland
[33] Horia Hulubei National Institute of Physics and Nuclear Engineering, Bucharest-Magurele, Romania
[34] Petersburg Nuclear Physics Institute (PNPI), Gatchina, Russia
[35] Institute of Theoretical and Experimental Physics (ITEP), Moscow, Russia
[36] Institute of Nuclear Physics, Moscow State University (SINP MSU), Moscow, Russia
[37] Institute for Nuclear Research of the Russian Academy of Sciences (INR RAS), Moscow, Russia
[38] Yandex School of Data Analysis, Moscow, Russia
[39] Budker Institute of Nuclear Physics (SB RAS), Novosibirsk, Russia
[40] Institute for High Energy Physics (IHEP), Protvino, Russia
[41] ICCUB, Universitat de Barcelona, Barcelona, Spain
[42] Instituto Galego de Física de Altas Enerxías (IGFAE), Universidade de Santiago de Compostela, Santiago de Compostela, Spain
[43] European Organization for Nuclear Research (CERN), Geneva, Switzerland
[44] Institute of Physics, Ecole Polytechnique Fédérale de Lausanne (EPFL), Lausanne, Switzerland
[45] Physik-Institut, Universität Zürich, Zürich, Switzerland
[46] NSC Kharkiv Institute of Physics and Technology (NSC KIPT), Kharkiv, Ukraine
[47] Institute for Nuclear Research of the National Academy of Sciences (KINR), Kyiv, Ukraine
[48] University of Birmingham, Birmingham, United Kingdom
[49] H.H. Wills Physics Laboratory, University of Bristol, Bristol, United Kingdom
[50] Cavendish Laboratory, University of Cambridge, Cambridge, United Kingdom

[51] *Department of Physics, University of Warwick, Coventry, United Kingdom*
[52] *STFC Rutherford Appleton Laboratory, Didcot, United Kingdom*
[53] *School of Physics and Astronomy, University of Edinburgh, Edinburgh, United Kingdom*
[54] *School of Physics and Astronomy, University of Glasgow, Glasgow, United Kingdom*
[55] *Oliver Lodge Laboratory, University of Liverpool, Liverpool, United Kingdom*
[56] *Imperial College London, London, United Kingdom*
[57] *School of Physics and Astronomy, University of Manchester, Manchester, United Kingdom*
[58] *Department of Physics, University of Oxford, Oxford, United Kingdom*
[59] *Massachusetts Institute of Technology, Cambridge, MA, United States*
[60] *University of Cincinnati, Cincinnati, OH, United States*
[61] *University of Maryland, College Park, MD, United States*
[62] *Syracuse University, Syracuse, NY, United States*
[63] *Laboratory of Mathematical and Subatomic Physics, Constantine, Algeria, associated to* [2]
[64] *Pontifícia Universidade Católica do Rio de Janeiro (PUC-Rio), Rio de Janeiro, Brazil, associated to* [2]
[65] *University of Chinese Academy of Sciences, Beijing, China, associated to* [3]
[66] *South China Normal University, Guangzhou, China, associated to* [3]
[67] *School of Physics and Technology, Wuhan University, Wuhan, China, associated to* [3]
[68] *Institute of Particle Physics, Central China Normal University, Wuhan, Hubei, China, associated to* [3]
[69] *Departamento de Fisica, Universidad Nacional de Colombia, Bogota, Colombia, associated to* [9]
[70] *Institut für Physik, Universität Rostock, Rostock, Germany, associated to* [13]
[71] *Van Swinderen Institute, University of Groningen, Groningen, Netherlands, associated to* [28]
[72] *National Research Centre Kurchatov Institute, Moscow, Russia, associated to* [35]
[73] *National University of Science and Technology "MISIS", Moscow, Russia, associated to* [35]
[74] *National Research Tomsk Polytechnic University, Tomsk, Russia, associated to* [35]
[75] *Instituto de Fisica Corpuscular, Centro Mixto Universidad de Valencia - CSIC, Valencia, Spain, associated to* [41]
[76] *University of Michigan, Ann Arbor, United States, associated to* [62]
[77] *Los Alamos National Laboratory (LANL), Los Alamos, United States, associated to* [62]

[a] *Universidade Federal do Triângulo Mineiro (UFTM), Uberaba-MG, Brazil*
[b] *Laboratoire Leprince-Ringuet, Palaiseau, France*
[c] *P.N. Lebedev Physical Institute, Russian Academy of Science (LPI RAS), Moscow, Russia*
[d] *Università di Bari, Bari, Italy*
[e] *Università di Bologna, Bologna, Italy*
[f] *Università di Cagliari, Cagliari, Italy*
[g] *Università di Ferrara, Ferrara, Italy*
[h] *Università di Genova, Genova, Italy*
[i] *Università di Milano Bicocca, Milano, Italy*
[j] *Università di Roma Tor Vergata, Roma, Italy*
[k] *Università di Roma La Sapienza, Roma, Italy*
[l] *AGH - University of Science and Technology, Faculty of Computer Science, Electronics and Telecommunications, Kraków, Poland*
[m] *LIFAELS, La Salle, Universitat Ramon Llull, Barcelona, Spain*
[n] *Hanoi University of Science, Hanoi, Vietnam*
[o] *Università di Padova, Padova, Italy*
[p] *Università di Pisa, Pisa, Italy*
[q] *Università degli Studi di Milano, Milano, Italy*
[r] *Università di Urbino, Urbino, Italy*
[s] *Università della Basilicata, Potenza, Italy*
[t] *Scuola Normale Superiore, Pisa, Italy*

[u] *Università di Modena e Reggio Emilia, Modena, Italy*
[v] *MSU - Iligan Institute of Technology (MSU-IIT), Iligan, Philippines*
[w] *Novosibirsk State University, Novosibirsk, Russia*
[x] *National Research University Higher School of Economics, Moscow, Russia*
[y] *Sezione INFN di Trieste, Trieste, Italy*
[z] *School of Physics and Information Technology, Shaanxi Normal University (SNNU), Xi'an, China*
[aa] *Physics and Micro Electronic College, Hunan University, Changsha City, China*
† *Deceased*